NASA TECHNICAL NOTE

NASA TN D-7359

NASA TN D-7359

CHARACTERISTICS OF CAPACITOR-TYPE MICROMETEOROID FLUX DETECTORS WHEN IMPACTED WITH SIMULATED MICROMETEOROIDS

by Philip C. Kassel, Jr.

Langley Research Center
Hampton, Va. 23665

NATIONAL AERONAUTICS AND SPACE ADMINISTRATION • WASHINGTON, D. C. • NOVEMBER 1973

1. Report No.	2. Government Accession No.	3. Recipient's Catalog No.
NASA TN D-7359		

4. Title and Subtitle	5. Report Date
CHARACTERISTICS OF CAPACITOR-TYPE MICROMETEOROID FLUX DETECTORS WHEN IMPACTED WITH SIMULATED MICROMETEOROIDS	November 1973
	6. Performing Organization Code
7. Author(s)	8. Performing Organization Report No.
Philip C. Kassel, Jr.	L-8962
	10. Work Unit No.
9. Performing Organization Name and Address	755-42-01-01
NASA Langley Research Center Hampton, Va. 23665	11. Contract or Grant No.
	13. Type of Report and Period Covered
12. Sponsoring Agency Name and Address	Technical Note
National Aeronautics and Space Administration Washington, D.C. 20546	14. Sponsoring Agency Code

15. Supplementary Notes

16. Abstract

A series of impact tests are described and data presented which characterize the operation of the capacitor-type micrometeoroid flux detectors used on the Meteoroid Technology Satellite (MTS). Capacitor-type detectors with silicon dioxide dielectric thicknesses of 0.4 and 1.0 μm were tested in the micrometeoroid impact simulator at the Langley Research Center, a 4-MV Van de Graaff electrostatic accelerator. The carbonyl iron projectiles were from 0.5 to 5.0 μm in diameter with velocities from 4 to 10.0 km/sec. The detector bias voltage was varied from -20 to -60 V; some tests were at detector temperatures of 90° C to -100° C; and the angle of impact varied from 0° to 75° from the normal to the detector.

These tests showed that (1) the detector operation is reliable when the bias voltage is greater than 30 V, (2) after an impact the detector returns to its original condition with an insignificant loss of active area, and (3) the sensitivity of the detector is inversely proportional to the detector thickness. The test results suggest a theoretical model in which the signal is an arc triggered by the impacting projectile, and the detector bias voltage must be high enough to insure that an arc will form.

17. Key Words (Suggested by Author(s))	18. Distribution Statement
Micrometeoroid detector – capacitor type Impact characteristics	Unclassified – Unlimited

19. Security Classif. (of this report)	20. Security Classif. (of this page)	21. No. of Pages	22. Price*
Unclassified	Unclassified	36	Domestic, $3.00 Foreign, $5.50

*For sale by the National Technical Information Service, Springfield, Virginia 22151

CHARACTERISTICS OF CAPACITOR-TYPE MICROMETEOROID FLUX DETECTORS WHEN IMPACTED WITH SIMULATED MICROMETEOROIDS

By Philip C. Kassel, Jr.
Langley Research Center

SUMMARY

A series of impact tests are described and data presented which characterize the operation of the capacitor-type micrometeoroid flux detectors used on the Meteoroid Technology Satellite (MTS). Capacitor-type detectors with silicon dioxide dielectric thicknesses of 0.4 and 1.0 μm were tested in the micrometeoroid impact simulator at the Langley Research Center, a 4-MV Van de Graaff electrostatic accelerator. The carbonyl iron projectiles were from 0.5 to 5.0 μm in diameter with velocities from 4 to 10.0 km/sec. The detector bias voltage was varied from -20 to -60 V; some tests were at detector temperatures of 90° C to -100° C; and the angle of impact varied from 0° to 75° from the normal to the detector.

These tests showed that (1) the detector operation is reliable when the bias voltage is greater than 30 V, (2) after an impact the detector returns to its original condition with an insignificant loss of active area, and (3) the sensitivity of the detector is inversely proportional to the detector thickness. The test results suggest a theoretical model in which the signal is an arc triggered by the impacting projectile, and the detector bias voltage must be high enough to insure that an arc will form.

INTRODUCTION

The meteoroid is one of the hazards of the space environment. To assess this hazard properly, many spacecraft missions have had as their primary or secondary objectives the measurement of meteoroids in near-Earth space. In spite of the many successes, the meteoroid environment is still not well known, especially with respect to the low-mass meteoroids, generally referred to as cosmic dust or micrometeoroids.

The most basic and probably the most important measurement made concerning meteoroids is a determination of the meteoroid flux – that is, the number of meteoroids encountered per unit area per unit time by a spacecraft in a particular orbit. Ideally, meteoroid flux should be measured as a function of the mass, density, velocity, or any

other characteristic of the meteoroids. Practically though, the flux can be measured as a function of the type of damage or hazard associated with the meteoroids counted. The pressurized cell, for example, has been used to measure fluxes of the larger meteoroids which represent a puncture hazard (ref. 1). However, puncture is not the only meteoroid hazard. Micrometeoroids which cannot penetrate the spacecraft can damage the surface. If such micrometeoroids exist in large numbers, they will limit the useful life of optical surfaces, windows, thermal balance coatings, or other spacecraft components that depend on fixed surface properties. To measure the flux of these micrometeoroids, a capacitor-type detector was developed for use on the Meteoroid Technology Satellite (MTS Explorer XLVI).

All three experiments of Explorer XLVI are designed to provide data describing the near-Earth meteoroid environment. The primary experiment uses pressurized cells to measure meteoroid penetration rates in a bumper-protected structure. A second experiment measures the velocity of meteoroids capable of penetrating a single sheet of stainless steel 12.7 μm thick. A third experiment measures the flux of micrometeoroids with a capacitor-type detector, the detector which is the subject of this report.

The capacitor-type meteoroid detector is a relatively simple device consisting of a parallel-plate capacitor with one plate exposed to the environment of space. The inner plate is voltage biased through a high resistance and when a meteoroid impacts the detector, a signal is obtained from this plate. The exact means by which an impacting meteoroid causes a signal is not clearly understood. However, it is generally accepted that if a meteoroid or projectile impacts the detector and forms a crater which extends from the outer plate through the dielectric and into the inner plate, such an impact should produce a signal which can be counted as a meteoroid encounter. Furthermore, after a signal is produced, the detector should revert to the original bias conditions and be able to detect additional meteoroids. To use a capacitor-type meteoroid impact detector in an experiment measuring meteoroid flux, there are two basic points to consider: qualification – the detector must operate reliably in the space environment – and calibration – its sensitivity must be known.

This report describes a series of impact tests which were part of the qualification test program for the micrometeoroid flux detector of Explorer XLVI. The primary purpose of these tests was to obtain data for an empirical description of the detector operation. These data were used to determine the optimum operating bias conditions and were helpful in designing the spacecraft circuit which would count the micrometeoroid impact signals. These tests also provided detector calibration data.

THE IMPACT DETECTOR

The capacitor-type micrometeoroid impact detector (fig. 1) is a product of metal-oxide-silicon (MOS) technology which is widely known for its role in the manufacture of field-effect transistors and integrated circuits. The detector is made from a 51-mm-diameter (2-in.) wafer of low-resistivity, p-type (boron-doped) silicon which forms the inner electrode of the capacitor. A layer of silicon dioxide (SiO_2) is grown on the wafer by thermal oxidation to form the dielectric of the capacitor. An aluminum coating is then vapor deposited on top of the SiO_2 to form the outer electrode. The capacitor is then electrically connected to a printed circuit board with 25-μm-diameter gold leads that are thermocompression bonded to each electrode. A cross section of the detector and the electrical circuit is shown in figure 2.

Micrometeoroid detectors having different sensitivities are obtained by using different thicknesses of the SiO_2 dielectric. Two detectors having different sensitivities were used for the micrometeoroid-flux-measuring experiment. The most sensitive detector (hereinafter referred to as the 0.4-μm detector) tested had an SiO_2 thickness of 0.4 μm and a capacitance of 0.165 μF. The less sensitive detector (hereinafter referred to as the 1.0-μm detector) had an SiO_2 thickness of 1.0 μm and a capacitance of 0.070 μF. These capacitor-type detectors were cleared to 80 and 120 V, respectively.

The clearing process described in reference 2 is a technique of neutralizing a type of defect that may exist in these capacitors. Such defects are localized and manifested by high or erratic leakage current. When the current through the defect is increased by increasing the bias voltage, the capacitor will discharge and dump its stored energy in the area of the defect. If this energy is sufficient, electrode material will be vaporized and removed from the area around the defect. If the energy is not too high, the defect will not be enlarged. Under these conditions the capacitor is cleared and exhibits the normal stable leakage currents, typically, 9 nA at -60 V bias for the 1.0-μm detector and 6 nA at -40 V bias for the 0.4-μm detector.

THE IMPACT FACILITY AND TEST INSTRUMENTATION

The micrometeoroid impact simulator at the Langley Research Center was used for the impact testing of the micrometeoroid detectors (ref. 3). This facility uses a 4-MV Van de Graaff generator to accelerate charged carbonyl iron projectiles of 0.5 to 5 μm in diameter to velocities over 10 km/sec. This facility was particularly suited for these tests since the mass of the projectiles (10^{-16} to 10^{-12} kg) was near the limit of the expected sensitivity range of the detectors. Another significant feature of this facility

was the absence of the gun debris and acceleration gases that occur in light-gas gun and exploding-wire accelerators. In the past, such facilities were used for impact testing of capacitor-type detectors but the test results were often difficult to interpret (ref. 4). The results of impact tests made with the electrostatic accelerator were expected to be highly consistent and lead to the development of a theoretical model that would explain the operation of the capacitor-type meteoroid detector.

The biggest advantage of the electrostatic accelerator is that the projectiles are charged and therefore easy to measure and control. After being accelerated by the Van De Graaff accelerator, the projectiles enter the instrumented control section (fig. 3) of the micrometeoroid impact simulator. In this section of the simulator, a computer controls the projectiles and records the measurements made on them. The time of flight for each projectile is measured over a 1.00-m flight path. If this time is within a preselected range, an electronic gate is opened to allow only that projectile to proceed to the target. For each projectile selected out of the many accelerated, three measurements are recorded: (1) the charge on the projectile, (2) the time of flight over a 1.00-m flight path, and (3) the acceleration voltage. From these three measurements, projectile parameters such as kinetic energy, velocity, mass, and momentum are calculated. The projectile diameter can also be calculated if the projectile is assumed to have a spherical shape and uniform density.

A detector mounted in the target chamber is shown in figure 4. The projectiles can be focused so that they impact in an area about 1 to 3 mm in diameter. The detector can be positioned vertically and horizontally with a precision of about 1 mm. The angle of projectile impact can be varied from 0° to 75° from the normal to the target. For normal impacts it is possible to have well-defined target areas about 5 to 7 mm in diameter. For thermal-environment impact tests, a target chamber with a heating element and liquid N_2 coils surrounding the detector was used. In such tests, the detector could not be moved, and electrostatic deflection plates were required to deflect the projectiles to impact different areas of the detector.

A schematic diagram of the instrumentation used to measure the detector signals is shown in figure 5 along with a sketch of a typical signal. The signal parameters of primary concern were the time of occurrence, the rise time, and the amplitude. The recovery time was less important because it is fixed by the RC time constant of the detector circuit, where R is the bias resistance (1 $M\Omega$) and C is the detector capacitance (0.070 or 0.165 μF). Recovery, itself, is more important than recovery time and a qualitative determination of the detector recovery was made by comparing the detector leakage current after a test to its magnitude before the test. If the leakage current is unchanged, the detector has recovered.

The two-beam oscilloscope (fig. 5) was the primary means of measuring the signal parameters and correlating the signal with the impacting projectile. The upper beam of the oscilloscope displayed the detector signal and was triggered by the electronic gate which selects projectiles to enter the target chamber. Thus the time of impact could be correlated with the occurrence of the detector output signal. The second beam of the oscilloscope was triggered by the detector signal and displayed the signal on a fast time base so that the signal rise time could be measured. The signal amplitude was measured from either of the scope traces or from the transient voltmeter. An event counter and a preliminary-design spacecraft circuit were used to count signals received from the detector. The vacuum tube voltmeter (VTVM) was used to measure the detector bias voltage. The nanoammeter and capacitance bridge could be switched into the circuit to measure the detector leakage current or capacitance.

IMPACT TESTS

The impact tests described in this report are divided into four series of tests that were performed while the detector was in the final stages of development. The first series of tests, designed to establish the relationship between detector bias voltage and signal levels, were on preliminary-design detectors. After these tests the detector manufacturing was changed to include a sintering process which causes the aluminum (outer electrode) to diffuse slightly into the silicon dioxide (dielectric) and provide a better bond between these capacitor elements. Because of this manufacturing change, the second series of tests on prototype detectors were a repeat of the first but with an improved test technique. The third and fourth series of tests were on detectors that were in every respect equivalent to detectors on the Explorer XLVI spacecraft. The third series of tests were at temperatures of 90° C and -100° C to insure that the detector would operate over the expected range of spacecraft temperatures. This series also included some tests at reversed-polarity bias to obtain further data on the operation of the detector. In the fourth series of tests the operation of the detector was observed at an expected threshold of sensitivity. Impact conditions which did not produce a signal were obtained by varying the angle of impact from 0° to 75° from the normal to the detector.

TEST RESULTS

The first series of tests were designed to evaluate the detector output signal and determine the relationship between this signal and the detector bias voltage. The series consisted of 16 tests of about 50 impacts each and one of 25 impacts, as listed in table I. Each test was conducted at a fixed bias voltage and at a particular detector target area.

In these tests the only restriction on projectiles was that the velocity be greater than 4.0 km/sec.

The signals received from the detector are classified according to amplitude into two types. Signals greater than 1 V are called discharge signals while those 1 V and less are called low-level signals. Although this classification may seem arbitrary, the difference between the two types of signals is substantial. Typical signals are shown in figure 6.

In figures 7 and 8 signal amplitude is plotted against detector bias voltage. As indicated in the figures, the discharge signals have been averaged for each test and show a strong relationship to the bias voltage. The low-level signals occurred only at bias voltages of 30 V and less. However, the signal amplitude varied from 500 mV down to the limit of detectability, which was about 5 mV. The individual tests in which no signals were observed have been omitted because, as will be shown later, it is not possible to be sure that a projectile impacted the detector.

To determine whether a relationship exists between the type of signals and the projectile parameters, the data of those tests which resulted in both types of signals (tests 5, 6, 11, and 12) are plotted in figures 9 to 12. In these figures each point represents an impacting projectile according to its velocity and diameter, and the plotting symbol indicates the type of signal obtained for that impact test. Points which indicate a projectile diameter of zero or greater than 5 μm are the result of an error in the charge measurement for those projectiles. There appears to be no correlation between signal type and projectile parameters for the 1.0-μm detector (figs. 9 and 10). However, for the 0.4-μm detector (figs. 11 and 12), the low-level signals occur mainly at the lower velocities. There is also some correlation between the no-signal events and irregularities in the facility operation.

An attempt was made to determine whether a projectile did impact the detector for the cases in which no signals were observed. The number of impacting projectiles for each test was determined by carefully studying each target area with a microscope and counting the number of craters. For tests in which there were only discharge signals, the number of craters equaled the number of signals (fig. 13(a)). When there were low-level signals, however, the number of craters found was less than the number of signals. Some craters were so small (less than 10 μm) that they could easily be overlooked. Although this microscopic search for craters could neither confirm nor deny the no-signal events, it did result in a significant observation about the discharge signals.

Figure 13(b) is a photomicrograph of an impact site where an impacting projectile caused a discharge signal. The damaged area of the impact site is nearly circular and the diameter varied from 85 to 10 μm depending on test conditions. Only the central part

(less than 10 μm in diameter) extends through the SiO_2 into the silicon, or inner conductor of the capacitor. In most of the area the aluminum (outer conductor) has been removed while the SiO_2 (dielectric) remains undamaged. Since the nature and extent of the damage cannot be attributed to the impacting projectile, the capacitor discharge (the discharge energy) must be responsible for some of this damage.

The relationship between the discharge signal and the damage area at the impact site is presented in figure 14. For each of the 17 tests in the series, the signal energy is plotted against damage area. The damage area A_d is calculated from the relation $A_d = \pi d^2/4$ where d is the average diameter of the damage at the impact sites. The detector signal energy E_s is calculated by subtracting from the detector energy before impact the energy remaining after the signal, or

$$E_s = \frac{1}{2} C V_b^2 - \frac{1}{2} C(V_b - V_s)^2$$

where C is the capacitance of the detector, V_b is the magnitude of the bias voltage, and V_s is the average signal voltage. For comparison, the maximum kinetic energy of the projectiles was 3 μJ, and their maximum cross-sectional area was 2×10^{-11} m^2.

The results of the second series of tests are summarized in table II. Although this series of tests were essentially a repeat of the first series, there were three important differences. First, the number of shots per test was reduced and the focusing of the accelerator was optimized to facilitate counting the craters for each test. Second, there were more shots at the expected flight bias voltage of -40 and -60 V for the 0.4- and 1.0-μm detectors, respectively. And third, an oscilloscope-camera was used to record the signal voltage for each shot.

The results of the second series of tests are essentially the same as those for the first test, but because of improvements in test technique some additional information was obtained. The oscilloscope traces indicate that the discharge signals are consistent and predictable. The discharge time, or rise time of the signals, was about 0.5 μsec for the 1.0-μm detector and about 1.5 μsec for the 0.4-μm detector.

The oscilloscope traces also permitted measurement of the amplitude of individual low-level signals. Figure 15 is a plot of signal amplitude against bias voltage. For this series of tests, the signal amplitude is plotted on a log scale so that the low-level signals can be included in the figure. The number of confirmed no-signal shots (obtained by subtracting the number of signals from the number of craters found for each test) is also included for this series.

The relationship between the type of signals and projectile parameters is similar to that found in the first series of tests. In this second series, however, there is the

additional information about the amplitude of the low-level signals. The results of the tests in which low-level signals occurred are presented in table III.

Typical photomicrographs of the detector damage in the second series of tests are shown in figure 16. In the upper photograph (fig. 16(a)), the damage resulting from an impact with low-level signal can be compared with that of an impact with discharge signal. When a low-level signal occurs, little or no aluminum is removed from around the impact site. The lower photograph (fig. 16(b)) is of the damage resulting from an impact with discharge signal when the bias is -60 V. This damage can be compared with that obtained under the same conditions in the first series of tests on a detector which was not sintered (fig. 13(b)). For the unsintered detector more aluminum was removed and the edge of the aluminum appears to have been peeled off the detector surface. Less aluminum was removed from the sintered detector and the edge of the aluminum looks as if it had been melted.

Figure 17 is a plot of the signal energy against damage area for the second series of tests. The dashed lines show the location of the points from the first series of tests (fig. 14). The solid line represents a constant ratio of signal energy to amount of aluminum removed (247 kJ/g). For comparison the minimum energy required to vaporize aluminum at room temperature is 10.6 kJ/g.

The third series of tests demonstrated that the detector would operate over a wide temperature range and that the polarity of the bias voltage does influence detector operation. The results of this series are presented in figures 18 to 20. In figure 18 the signal amplitude is plotted against bias voltage. Each point is an average for five impacts, and the dashed bars indicate the range of data from the second series of tests, which were at room temperature.

Photomicrographs of the impact sites in this series of tests showed some interesting variations in the shape of the damaged area (figs. 19 and 20). Figure 19 shows four of five impact sites for one test at -60° C and figure 20 shows typical impact sites which occurred when there was positive-polarity bias on the silicon (inner) electrode. The effect of bias polarity on the damage area is seen by comparing figure 20(a) with figure 16(b). Although the signal level and energy are less for positive bias, the damage area is larger and the edge of the aluminum around the area is uneven. These differences occur because the aluminum, depending on the polarity of the bias, is the anode or cathode for the discharge signal.

The fourth series of tests were the only ones to show any difference in sensitivity between the 1.0- and 0.4-μm detectors when operated at the expected flight bias voltage. In this series of tests, there were 80 impacts in each thickness of detector. All impacts were at a bias of -60 V for the 1.0-μm detector and -40 V for the 0.4-μm detector. In

these tests the normal component of the projectile velocity was controlled by varying the impact angle from 0^{o} to 75^{o} from the normal to the detector. The results of the tests are plotted in figures 21 and 22. In figure 21 the projectiles impacting the 1.0-μm detector are plotted according to diameter and the computed normal velocity. The projectiles which caused a discharge signal are plotted as open symbols and those which did not cause a signal, as solid symbols. There were no low-level signals. The line in the figure indicates the threshold of sensitivity. With few exceptions, projectiles with parameters above or to the right of the line produced signals while those below or to the left did not. In a similar manner the data for the 0.4-μm detector are plotted in figure 22 and the threshold for the 1.0-μm detector is included in this figure for comparison.

In these figures the lines which indicate the extent of the detector sensitivity have been constrained not only to fit the data but also to be consistent with one another (parallel) and have some physical significance. These lines represent projectiles which have a constant value of dv^2, where d is projectile diameter and v is normal velocity. Thus, $dv^2 = 5.62\ m^3/sec^2$ is the lower limit of sensitivity for the 1.0-μm detector to carbonyl iron projectiles, and $dv^2 = 2.81\ m^3/sec^2$ is the lower limit for the 0.4-μm detector. It is interesting to note that the ratio of the sensitivites indicated by the lines is 2.0, which is approximately the ratio of the effective thickness of the detectors (dielectric plus outer electrode).

DISCUSSION

Both the 0.4- and 1.0-μm detectors will function as micrometeoroid impact detectors over a wide range of temperatures (-100^{o} C to 95^{o} C). When the detector is impacted by a projectile, a signal is obtained which is strongly dependent on the bias voltage. When the magnitude of the bias voltage is greater than 30 V, the operation of the detector is very consistent; the signal is always greater than 10 V and can best be described as a capacitor discharge. With a bias voltage of -20 V, most of the signals are low level and range from a few tenths of a volt down to a few millivolts, with some impacts producing no detectable signal. With a bias voltage between -20 and -30 V, an impact may result in either of these two types of signals.

When a discharge signal occurs, the self-clearing feature of the detector can be observed. The discharge of the detector takes place at the point of impact and is never complete but stops when the voltage on the detector has been reduced to between 20 and 10 V. The energy associated with this capacitor discharge, approximately 0.1 mJ, is sufficient to vaporize the aluminum electrode in a circular area centered at the impact site. The amount of aluminum removed or the area cleared is proportional to the discharge energy and is approximately $1.5 \times 10^{-8}\ m^2$ or 1.3 millionths of the total detector area.

When there is a low-level or millivolt signal, no self-clearing occurs. Occasionally a low-level signal is followed by increased or erratic detector leakage current.

The test which demonstrated the difference in sensitivity of the two detectors can only be considered a preliminary calibration because the significant data of these tests were for impacts that were from 60° to 75° from the normal to the detector. At such large angles it is difficult to ensure that the projectiles are impacting the detector; thus, the tests which result in no signals are not as significant as those that do produce signals. The large impact angles of these tests also bring out a more subtle difficulty with the calibration of these detectors.

In the calibration plots of figures 19 and 20, the effect of changing the impact angle is assumed to be equivalent to reducing the velocity of the projectile by the factor cos θ, where θ is the incident angle measured from the normal. For the calibration to be valid, this assumption must be valid even to angles as extreme as 75°. In questioning the validity of this assumption, one faces the real difficulty in calibrating a capacitor-type impact detector. To determine the validity of such an assumption, there must be some understanding of the process by which an impacting projectile causes a signal. Without this knowledge, the results of laboratory impact tests cannot be extrapolated to imply a calibration over the meteoroid spectrum.

Finally, some conclusion can be made concerning the process by which a projectile causes a signal. All the test results can be accounted for by explaining this process in terms of a theoretical model with two premises: First, the impacting projectiles trigger an arc, and second, the arc discharges the capacitor.

This model suggests that for counting micrometeoroids, the detector bias should be high enough to ensure that an arc will form. At the higher bias voltages, there is a predictable high-level signal which is easily counted. Also, the arc provides the highly desirable, self-clearing feature. For calibration tests, however, the model is useful in formulating some questions which have not been answered by these tests. For example, (1) What is the current density that can occur in the dielectric without triggering an arc? (2) Would such a trigger level be a useful measure of the detector sensitivity? and (3) Is the electric field strength as important as the dielectric thickness in determining the detector sensitivity? These questions define areas for future research studies for this type of detector.

CONCLUSIONS

An investigation has been conducted in which 0.5- to 5-μm-diameter carbonyl iron spheres traveling at velocities of 4 to 10 km/sec impacted metal-oxide-silicon, capacitor-type, micrometeoroid flux detectors such as those flown on the Meteoroid Technology Satellite. On the basis of the extensive test results, the following conclusions are drawn:

1. With a negative bias voltage greater than 30 V, the operation of the detectors is reliable and predictable. The signals obtained are capacitor discharge signals with a rise time of about 1 μ sec and a peak signal greater than 10 V.

2. The self-clearing feature of the detector is accomplished by the removal of outer electrode material from an area surrounding the impact site. The amount of material removed is proportional to the capacitor discharge energy but does not represent a significant loss of detector area.

3. A difference in sensitivity was observed for detectors with dielectric thicknesses of 0.4 and 1.0 μm when impacted at angles of incidence of 60° to 75° from the normal. The sensitivity is inversely proportional to the total thickness of the dielectric and outer electrode.

4. The data suggest a theoretical model of operation in which the impacting projectile triggers an arc and the arc in turn discharges the capacitor. The capacitor discharge can be observed as the detector signal when the bias is high enough to ensure that the arc will form.

Langley Research Center,
National Aeronautics and Space Administration,
Hampton, Va., August 27, 1973.

REFERENCES

1. D'Aiutolo, C. T.; Kinard, W. H.; and Naumann, R. J.: Recent NASA Meteoroid Penetration Results From Satellites. Meteor Orbits and Dust, Gerald S. Hawkins, ed., NASA SP-135, pp. 239-251.

2. Canady, K. S.; Monteith, L. K.; and Donovan, R. P.: Characterization of Silicon Oxide for a Capacitance-Type Meteoroid Penetration Detector. Contract No. NAS1-7949, Res. Triangle Inst., Sept. 1968. (Available as NASA CR-66712.)

3. Golub, Robert A.; and Davidson, John R.: Micrometeoroid Impact Simulation System. Space Simulation, J. C. Richmond, ed., NBS Spec. Publ. 336, Oct. 1970, pp. 915-933.

4. Broderick, John J.: Capacitor-Type Meteoroid-Penetration Sensors – Description and Test Results. NASA TN D-4524, 1968.

TABLE I.- RESULTS OF FIRST SERIES OF IMPACT TESTS TO DETERMINE RELATION BETWEEN DETECTOR (UNSINTERED) BIAS AND SIGNAL VOLTAGES

[Impacting particles were 0.5- to 5-μm-diameter carbonyl iron spheres traveling at over 4 km/sec]

Test	Detector number	Detector thickness, μm	Detector bias, V	Number of shots	Number of discharge signals	Av amplitude of discharge signals, V	Number of low-level signals	Number of shots resulting in no signal
1	2-4	0.4	-50	51	48	39.3	0	3
2			-45	50	49	32.7	0	1
3			-40	50	49	26.7	0	1
4			-35	50	42	20.2	0	8
5			-30	51	42	15.3	7	2
6			-25	50	29	9.1	18	3
7			-20	25	2	2.1	19	4
8	5-10	1.0	-45	50	43	29.1	0	7
9			-40	50	45	24.4	0	5
10			-35	50	45	19.0	0	5
11			-30	50	35	13.0	5	10
12			-25	50	13	7.3	26	11
13	11-10	1.0	-60	52	49	50.7	0	3
14			-55	50	48	43.7	0	2
15			-50	51	44	37.7	0	7
16			-45	50	43	31.2	0	7
17			-40	50	37	25.4	0	13
18	4-4	0.4	-40	(*)	1	26.0		

*Detector shorted within a few seconds when impacted at a rate of 60 impacts per second.

TABLE II.- RESULTS OF SECOND SERIES OF IMPACT TESTS (SINTERED DETECTORS)

[Impacting particles were 0.5- to 5-μm-diameter carbonyl iron spheres traveling at over 4 km/sec]

Test	Detector number	Detector thickness, μm	Detector bias, V	Number of shots	Number of discharge signals	Number of low-level signals	Number of shots resulting in no signal	Number of craters	Average damage area, m^2
18	21-10	1.0	-60	40	38	0	2	38	19.6×10^{-10}
19	17-4	0.4	-40	20	20	0	0	20	16.5×10^{-10}
20			-40	20	16	0	4	16	15.6
21			-35	10	9	0	1	9	12.2
22			-30	10	8	0	2	8	10.2
23			-25	10	6	3	1	9	5.43
24			-20	10	1	5	4	8	3.14
25	20-10	1.0	-60	11	7	0	4	7	
26			-60	11	10	0	1	10	19.6×10^{-10}
27			-60	10	7	0	3	7	18.1
28			-50	10	10	0	0	10	13.2
29			-40	11	10	0	1	10	8.29
30			-30	10	8	1	1	9	4.71
31			-25	11	5	5	1	11	3.14
32			-20	9	1	7	1	8	3.14
33	16-4	0.4	-40	10	10	0	0	10	18.8×10^{-10}
34			-40	10	10	0	0	10	19.2
35			-40	10	10	0	0	10	16.6
36			-40	10	10	0	0	10	17.4

TABLE III.- RESULTS OF INDIVIDUAL IMPACT TESTS THAT ILLUSTRATE THE GENERATION OF BOTH DISCHARGE AND LOW-LEVEL SIGNALS

Test	Detector number	Detector thickness, μm	Detector bias, V	Projectile diameter, μm	Projectile velocity, km/sec	Signal amplitude, V
23	17-4	0.4	-25	0.712	8.66	0.000
				.808	9.02	8.5
				.920	8.16	8.5
				1.01	8.05	9.5
				1.14	6.98	11.5
				1.14	6.89	8.5
				1.29	6.49	9.5
				1.35	6.52	.080
				1.91	5.04	.200
				3.02	4.35	.350
24	17-4	0.4	-20	0.868	8.36	0.000
				1.08	7.23	.000
				1.08	7.10	.000
				1.32	6.36	8.0
				1.38	6.66	.020
				1.40	6.01	.000
				1.53	5.91	.040
				1.93	5.37	.020
				2.02	5.05	.020
				2.04	5.08	.040
30	20-10	1.0	-30	0.579	9.73	14.5
				.730	8.41	13.5
				.734	8.78	.020
				.944	7.83	.000
				.994	7.88	17.5
				1.03	7.51	13.5
				1.56	5.76	16.0
				1.63	5.83	15.5
				1.64	5.76	13.0
				1.92	5.30	16.5
31	20-10	1.0	-25	0.529	10.1	0.005
				.714	9.12	.020
				.852	8.00	.000
				.908	8.07	9.5
				.972	7.73	8.5
				1.00	7.35	9.0
				1.47	6.27	9.5
				1.50	6.27	10.0
				1.88	4.54	.080
				1.92	5.15	.440
				2.65	4.44	.120
32	20-10	1.0	-20	0.642	9.57	0.000
				1.01	7.61	.080
				1.06	7.14	.030
				1.19	6.66	.010
				1.22	7.09	9.0
				1.22	6.55	.060
				1.28	6.58	.020
				1.34	6.24	.005
				1.67	5.64	.005

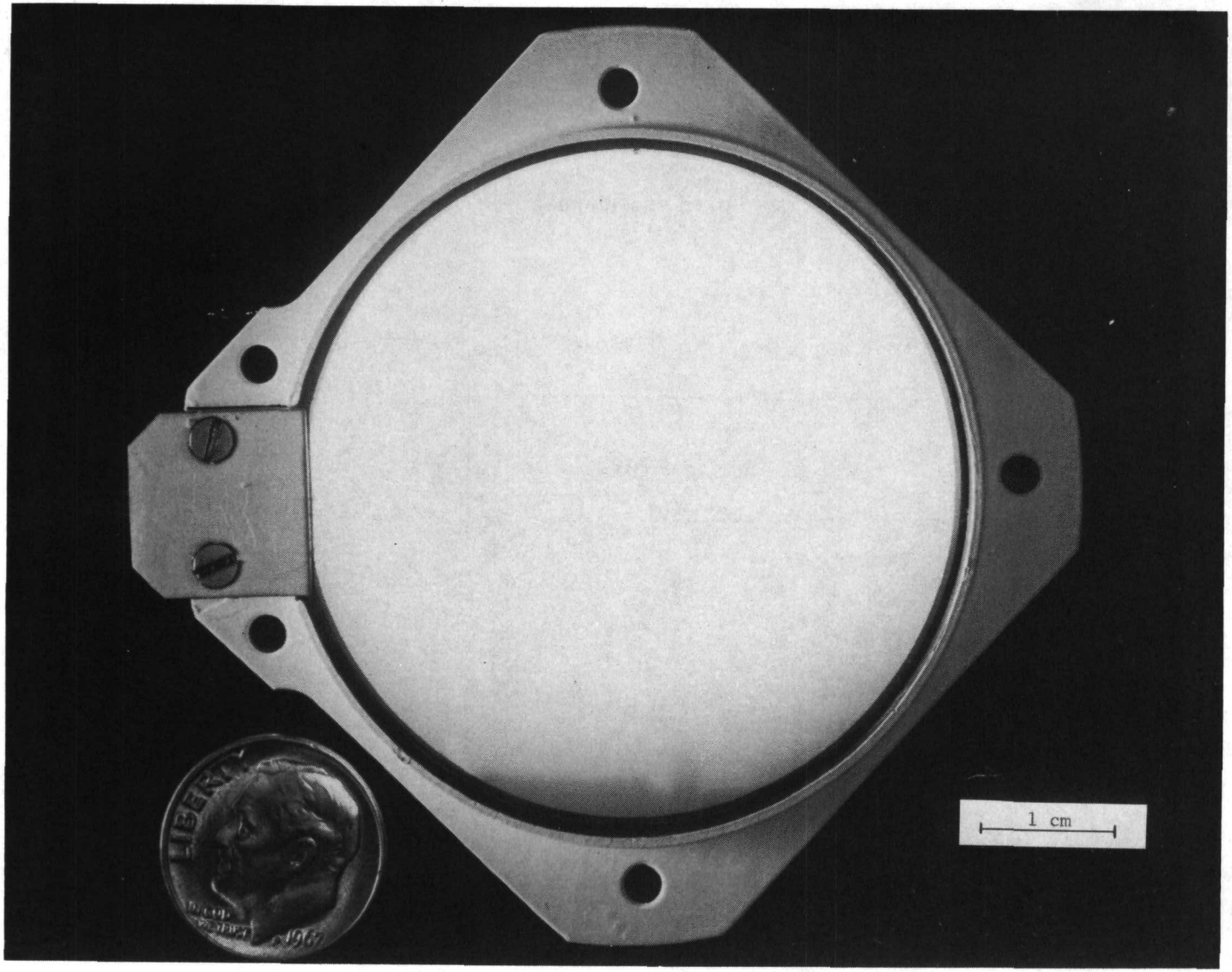

L-70-3044.1

Figure 1.- Micrometeoroid impact detector used on the Meteoroid Technology Satellite (Explorer XLVI).

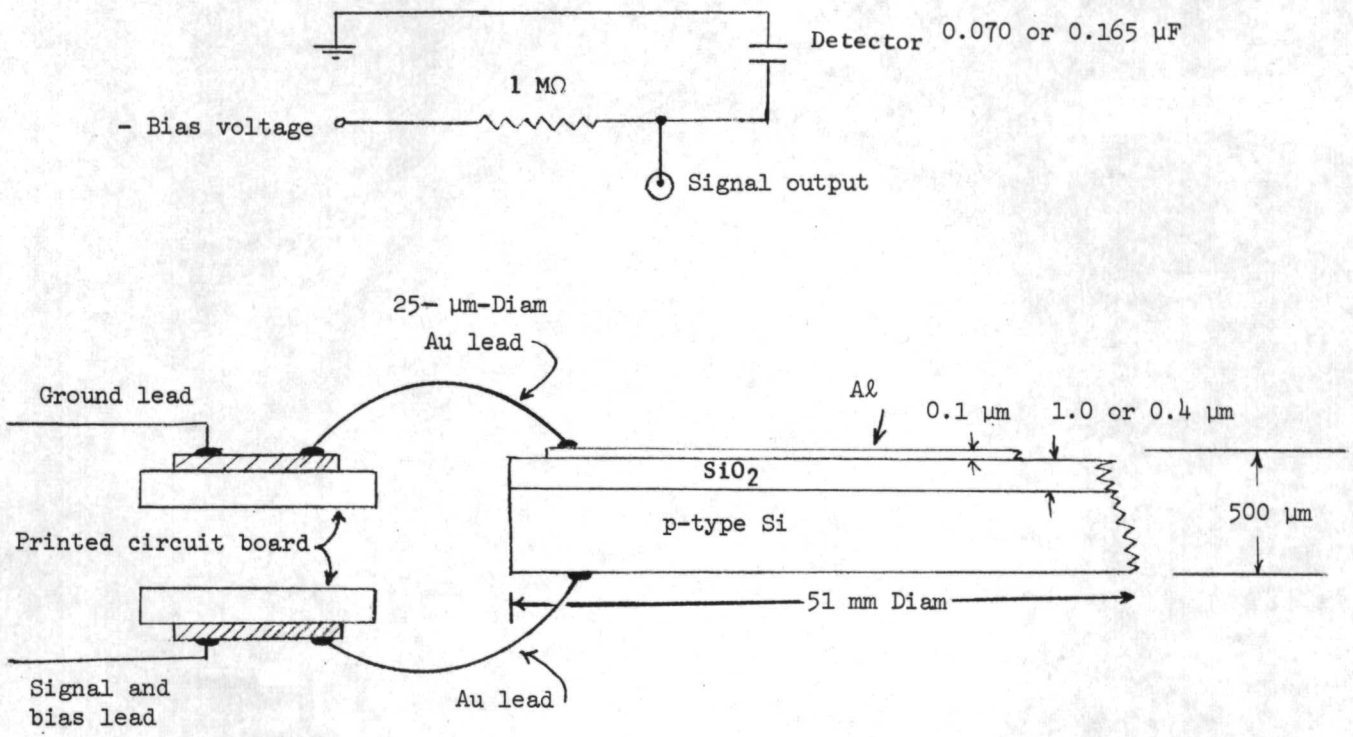

Figure 2.- Details of the electrical connections to the MOS micrometeoroid detector.

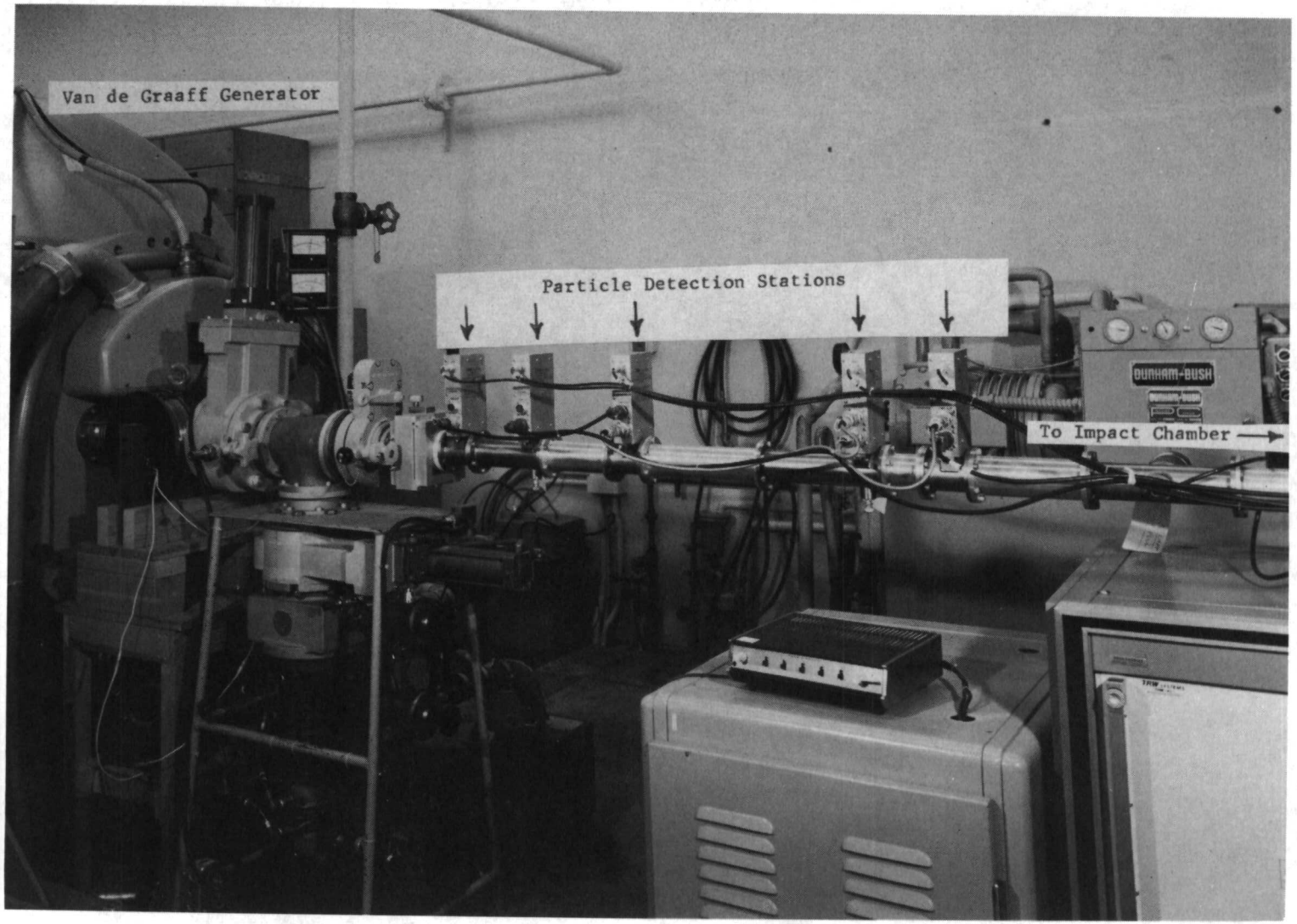

L-71-7744.1

Figure 3.- Projectile measurement and control section of the micrometeoroid impact simulator at the Langley Research Center.

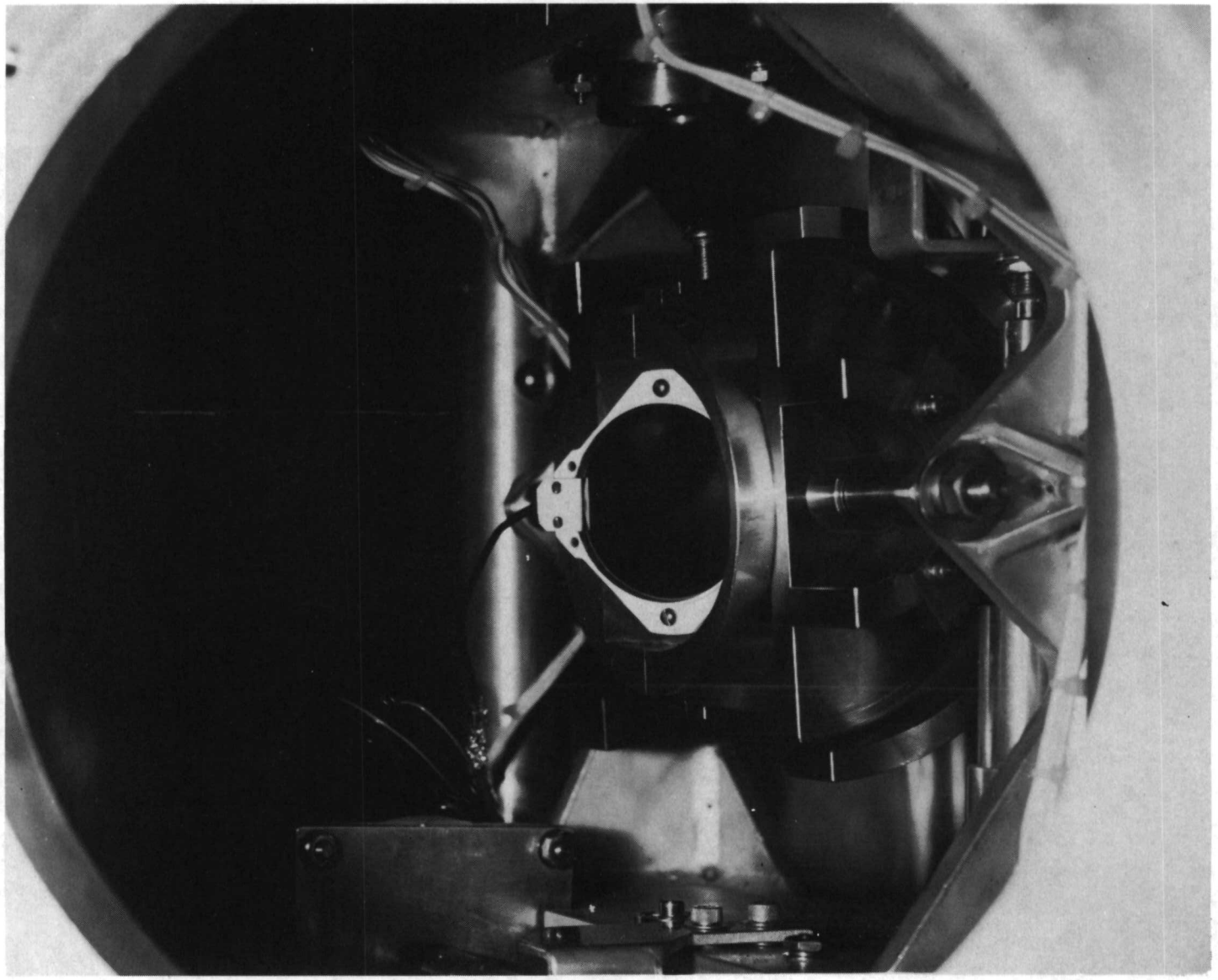

L-71-7745

Figure 4.- Micrometeoroid impact detector in the target chamber of the micrometeoroid impact simulator.

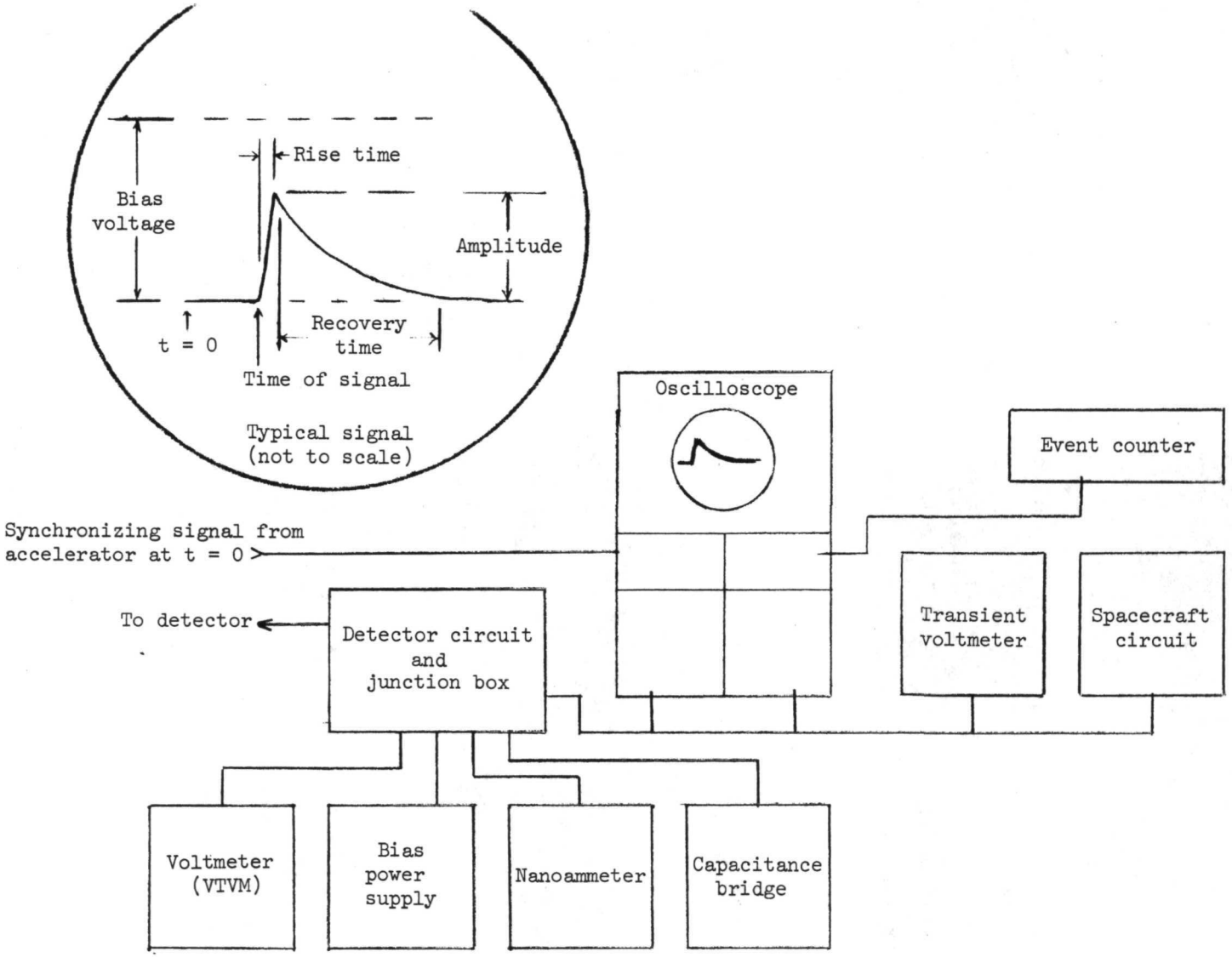

Figure 5.- Block diagram of instrumentation used to measure detector signals.

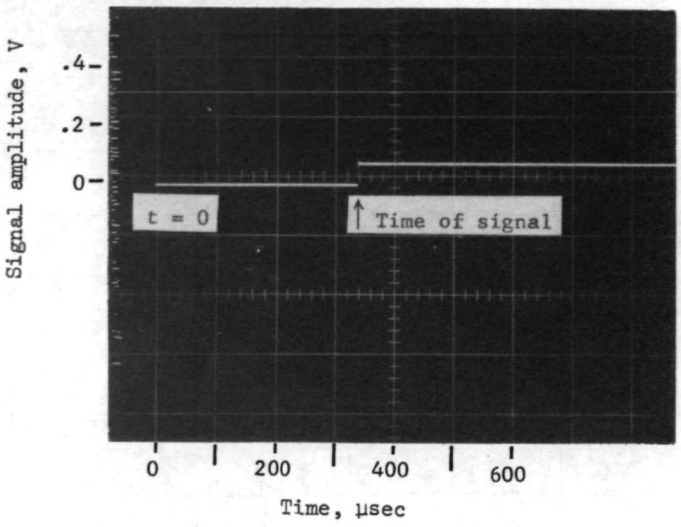

Detector thickness: 1.0 μm
Bias: -20 V
t = 0: projectile at electrostatic gate
Distance from gate to target: 2.57 m
Projectile velocity: 7.61 km/sec
Calculated time of impact: 338 μsec
Time of signal: 340 μsec
Signal amplitude: 80 mV

(a) Low-level signal.

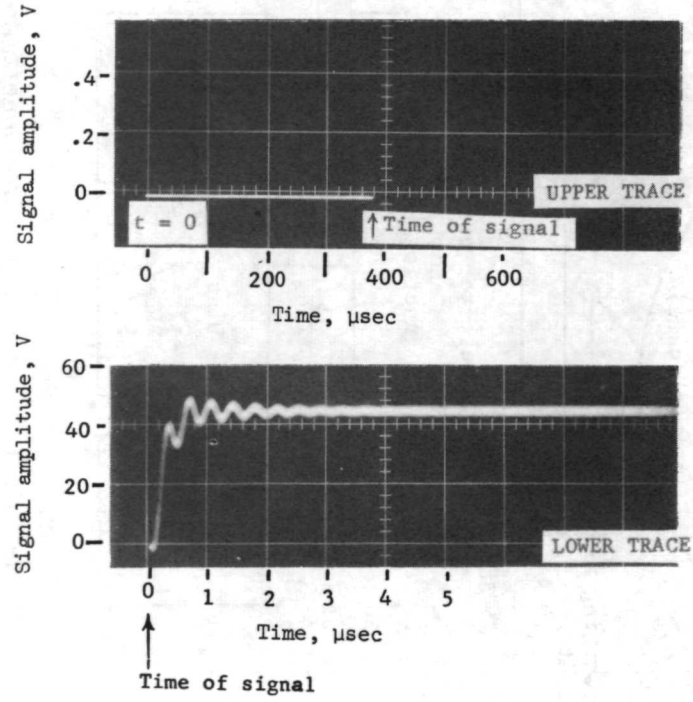

Detector thickness: 1.0 μm
Bias: -60 V
Projectile velocity: 6.79 km/sec
Calculated time of impact: 378 μsec
Time of signal: 380 μsec
Signal amplitude: 45 V

L-73-6826

(b) Discharge signal.

Figure 6.- Typical oscilloscope data for low-level and discharge signals.

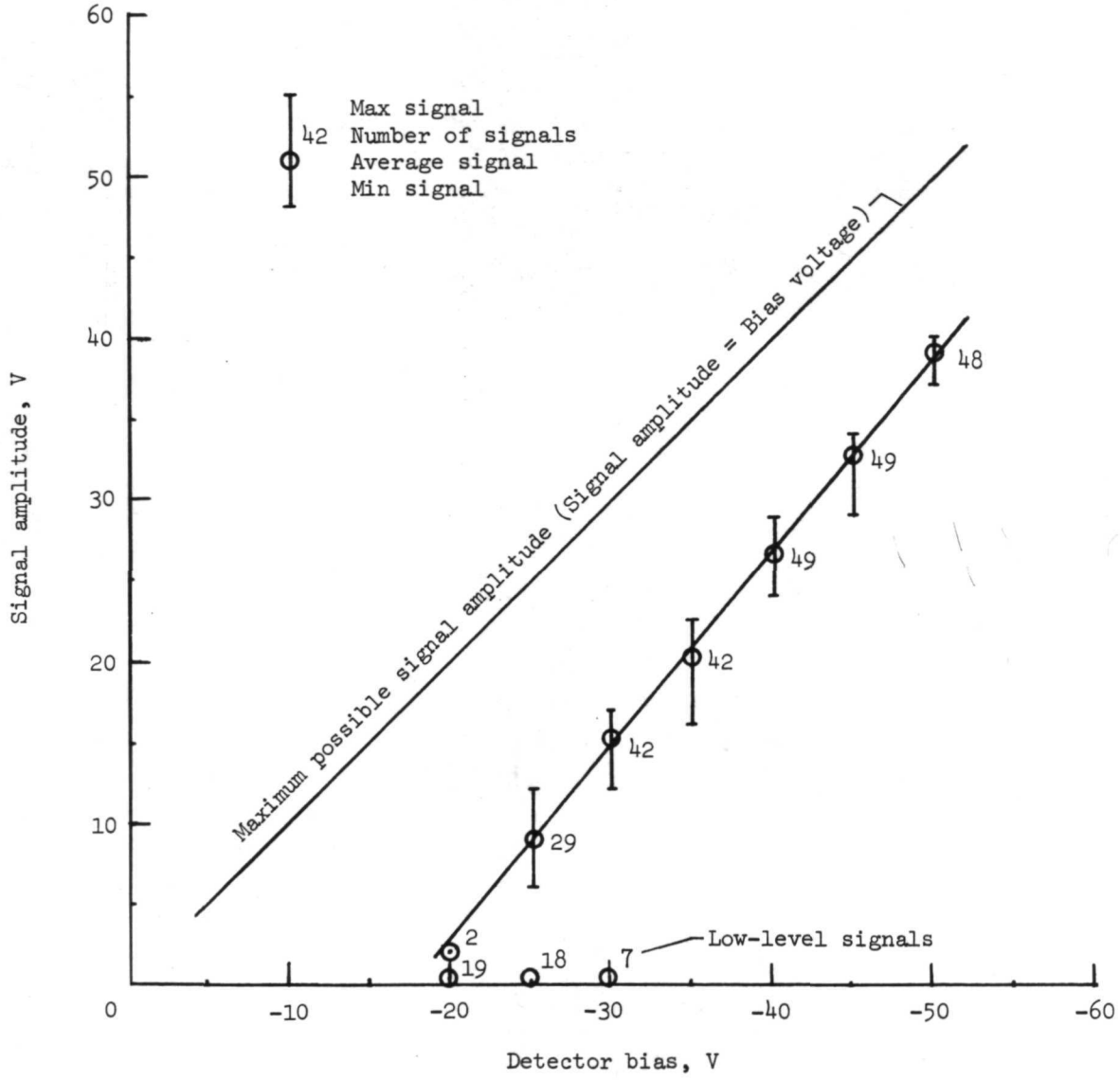

Figure 7.- Signal amplitude versus bias voltage for detector with a dielectric thickness of 0.4 μm. Tests 1 to 7.

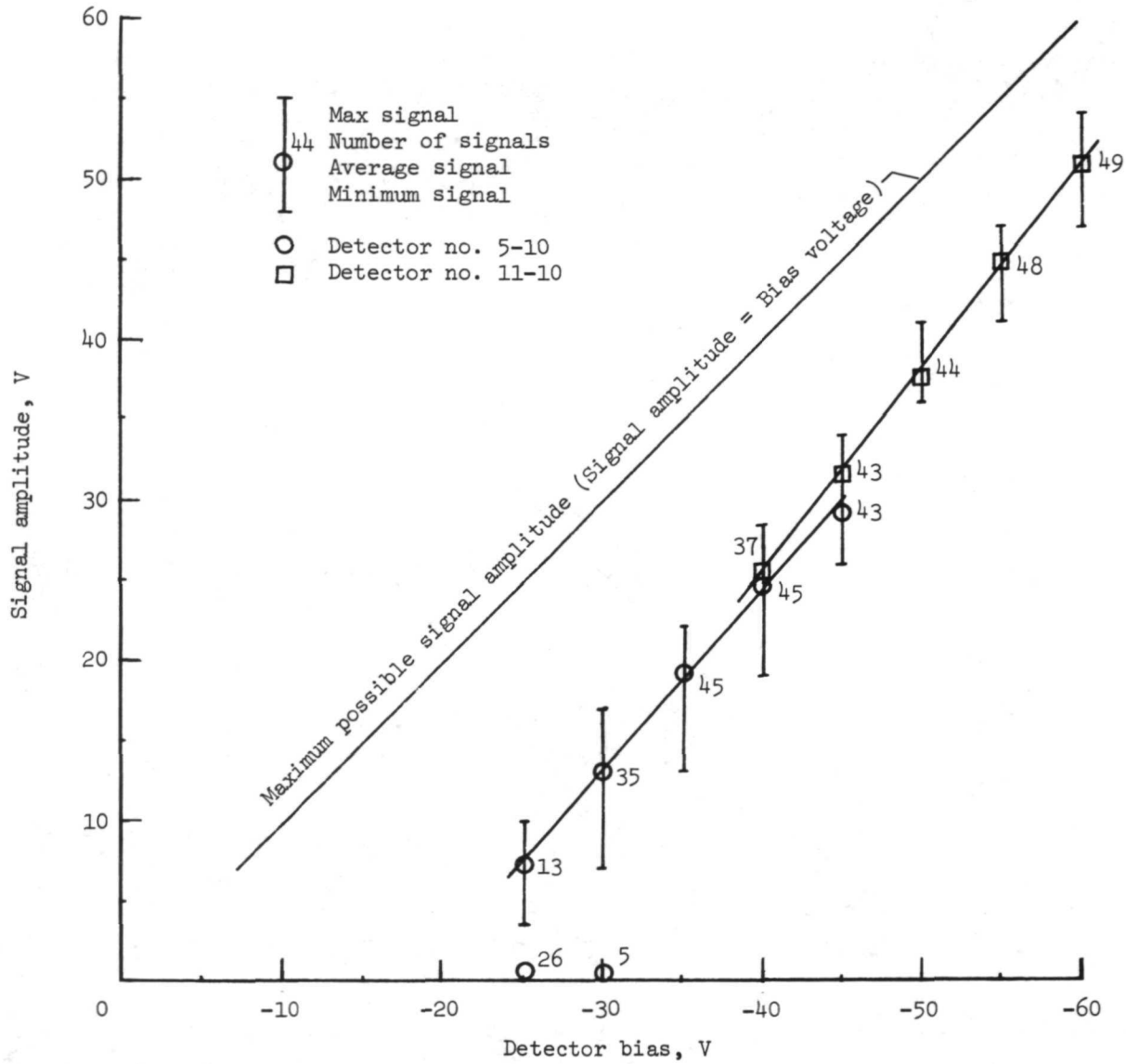

Figure 8.- Signal amplitude versus bias voltage for detector with a dielectric thickness of 1.0 μm. Tests 8 to 17.

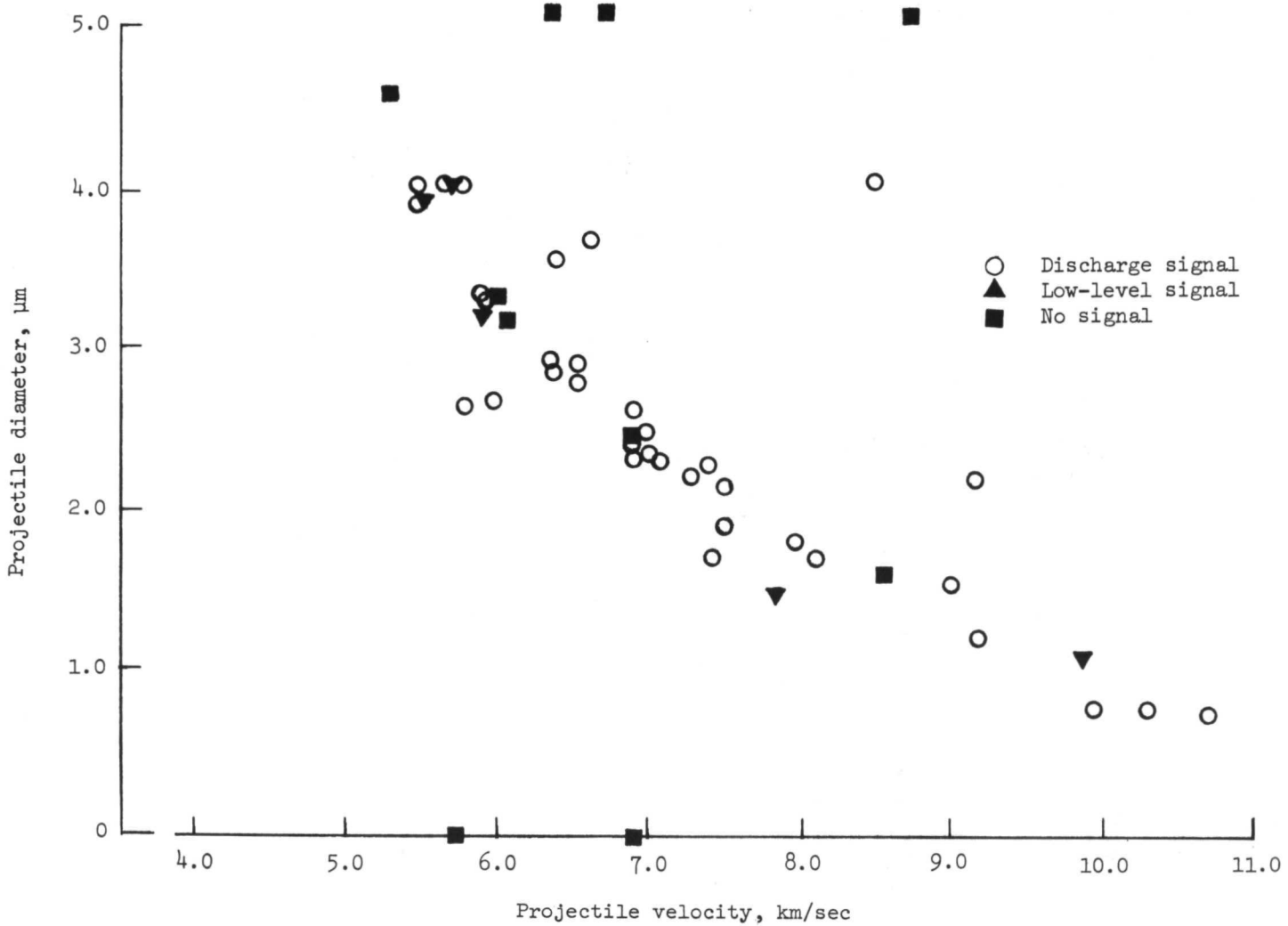

Figure 9.- Correlation between projectile parameters and type of signals for 1.0-μm detector at bias of -30 V. Test 11.

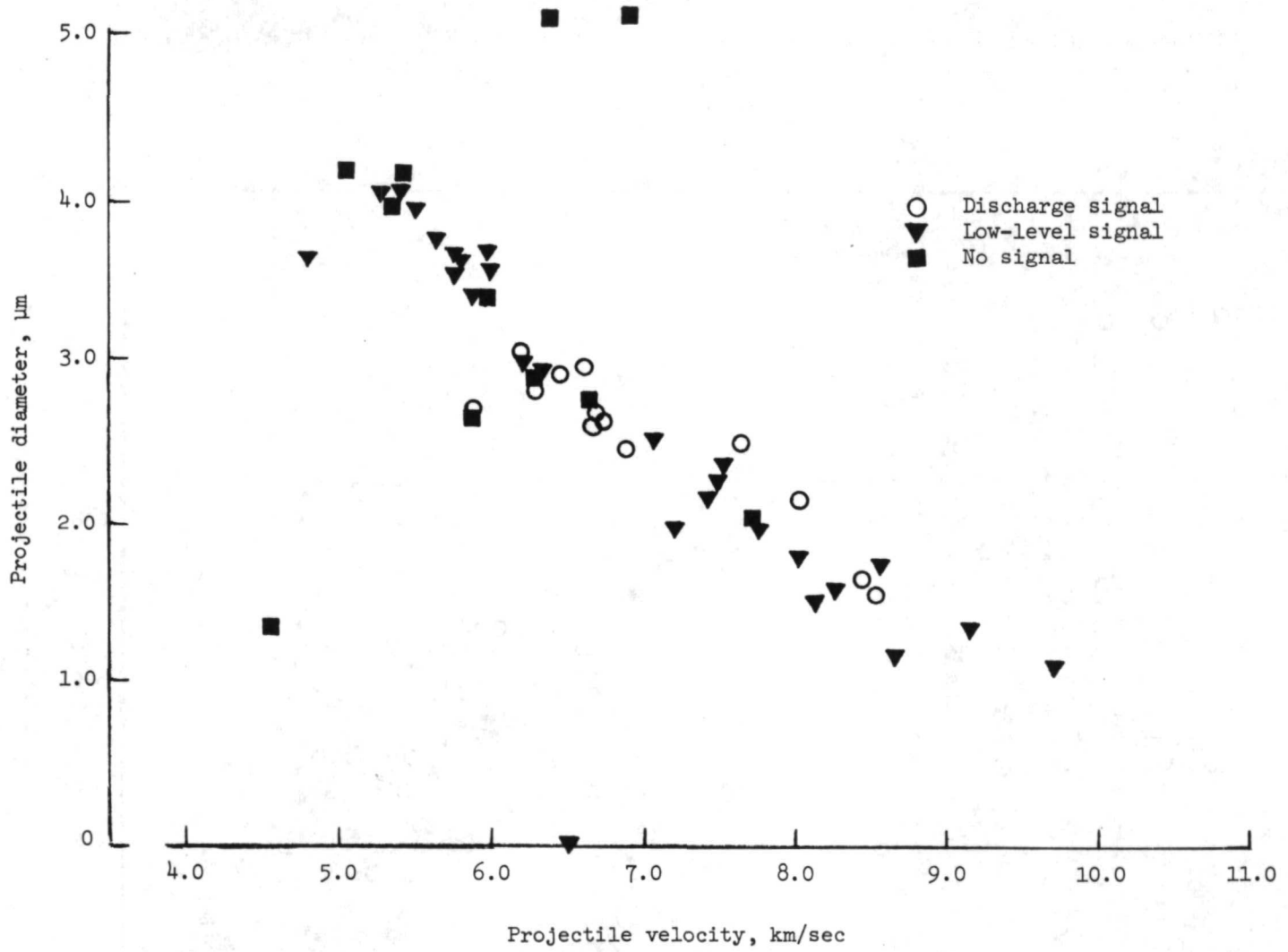

Figure 10.- Correlation between projectile parameters and type of signals for 1.0-μm detector at bias of -25 V. Test 12.

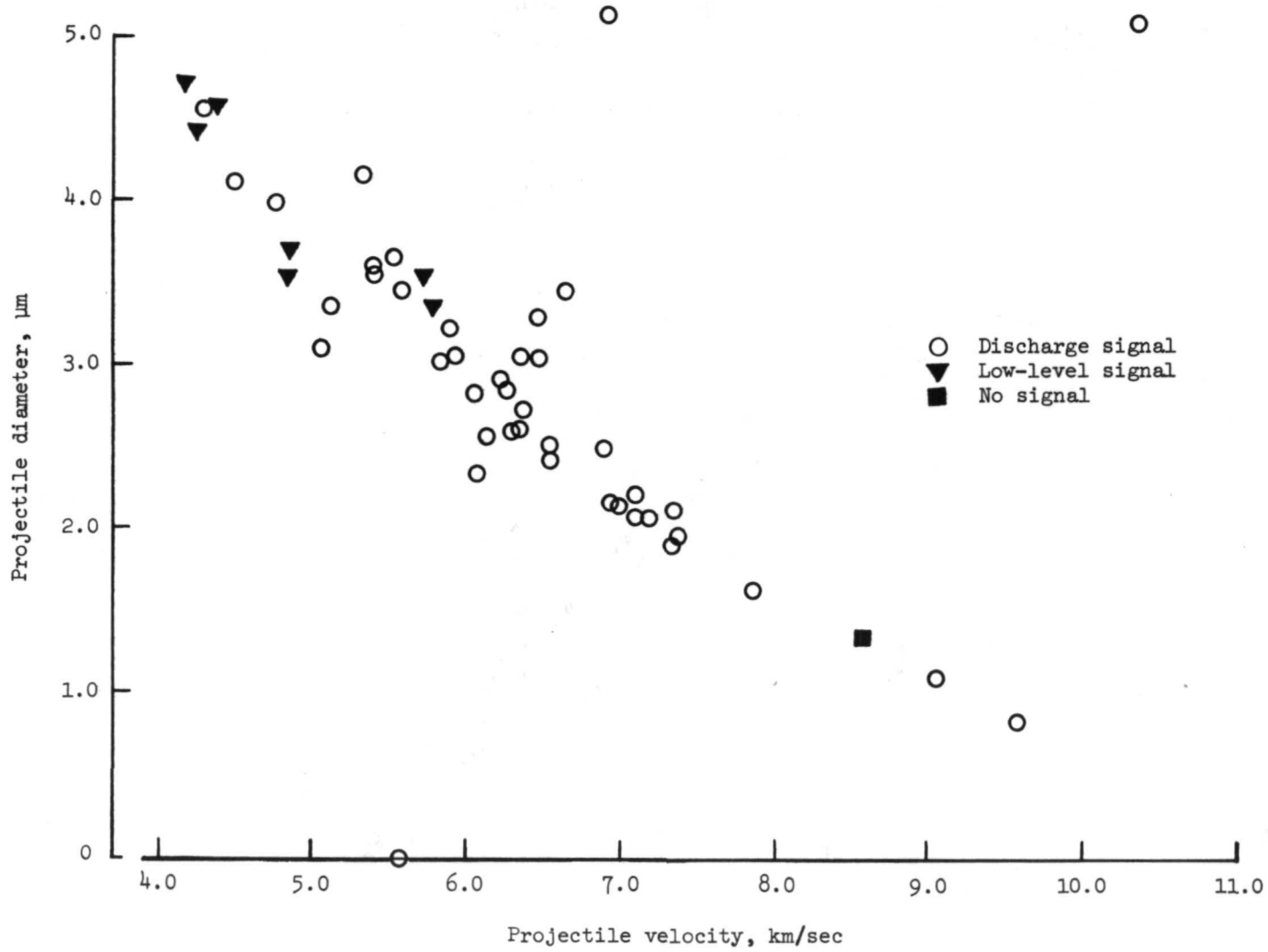

Figure 11.- Correlation between projectile parameters and type of signals for 0.4-μm detector at bias of -30 V. Test 5.

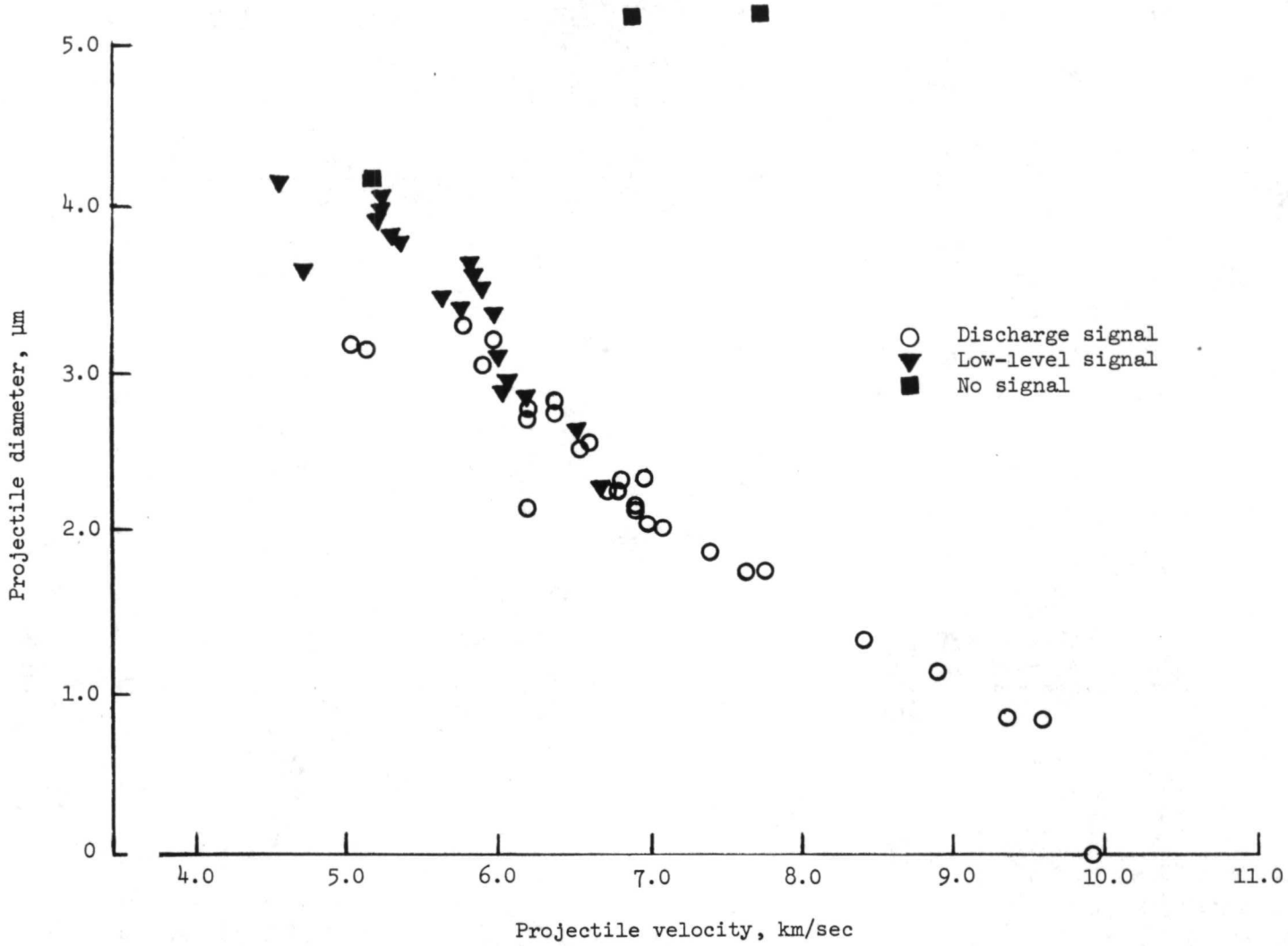

Figure 12.- Correlation between projectile parameters and type of signals for 0.4-μm detector at bias of -25 V. Test 6.

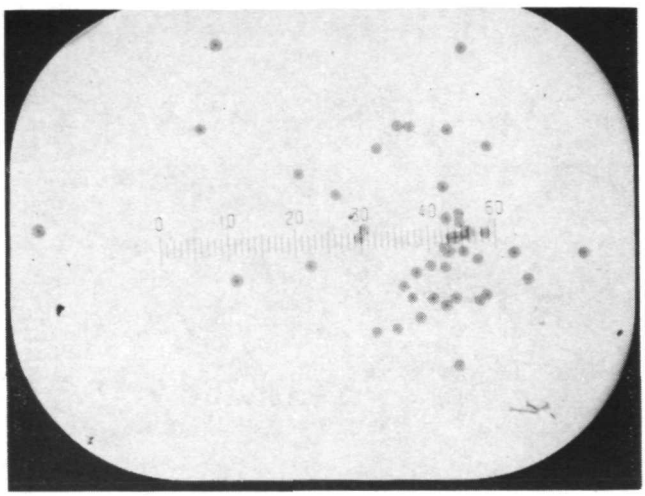

(a) Typical detector target area. Scale: 1 division = 25 μm; test 8; bias, -45 V; 1.0-μm detector.

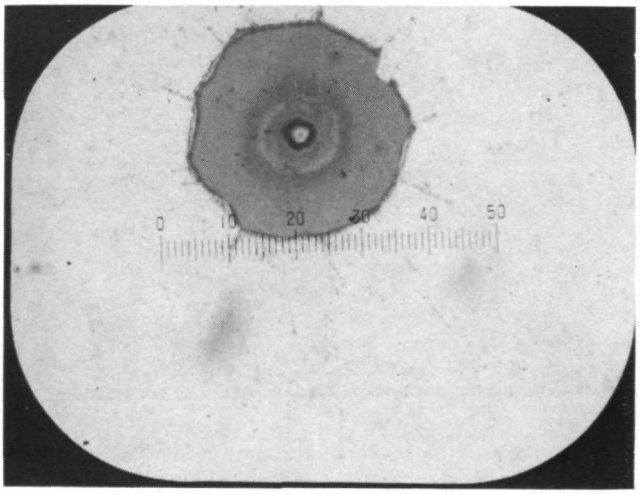

L-73-6827

(b) Typical impact-signal crater. Scale: 1 division = 2.5 μm; test 13; bias, -60 V; 1.0-μm detector.

Figure 13.- Photomicrographs of impact sites on a micrometeoroid detector.

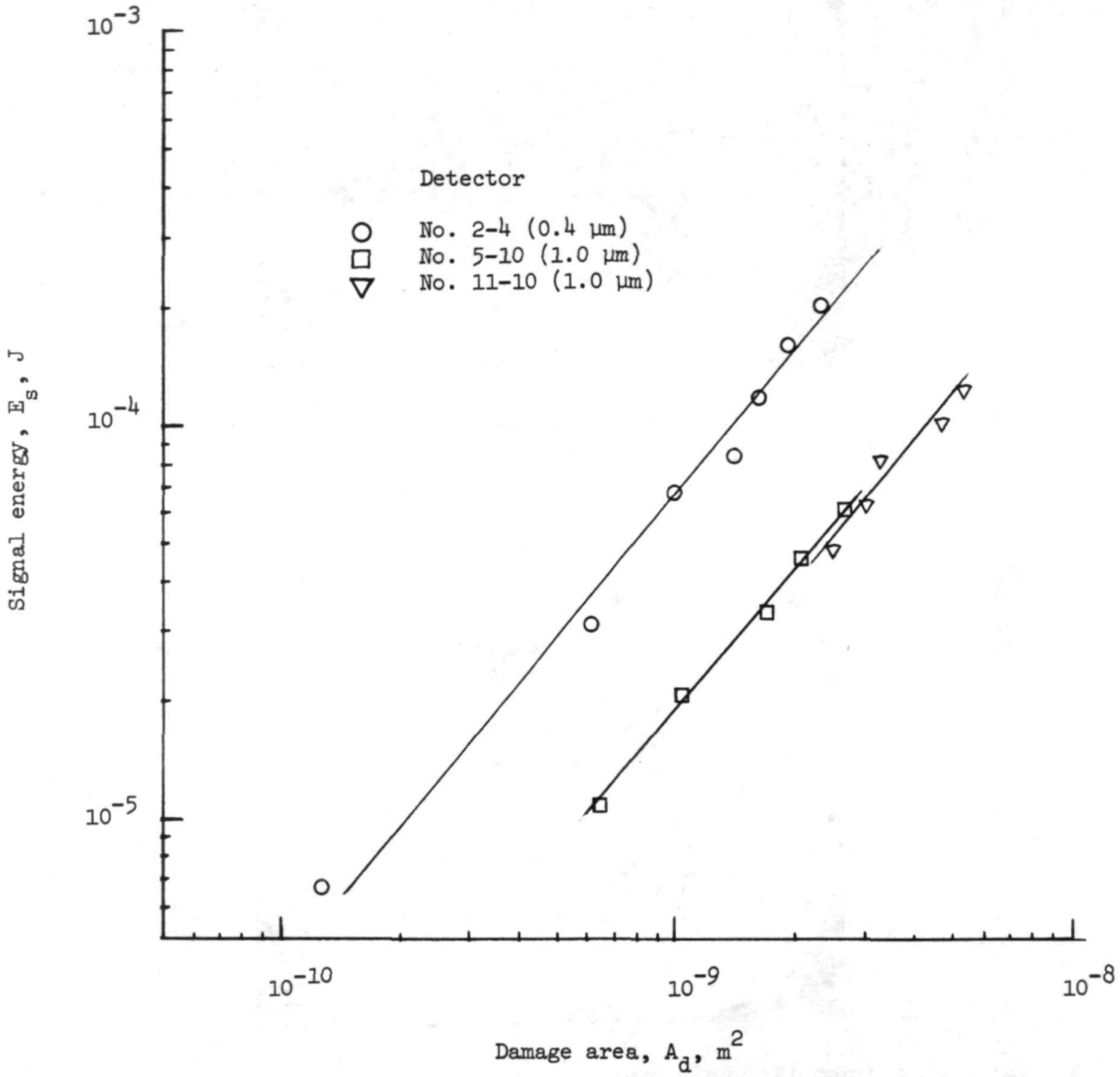

Figure 14.- Correlation of signal energy with damage area at the impact site. Tests 1 to 17.

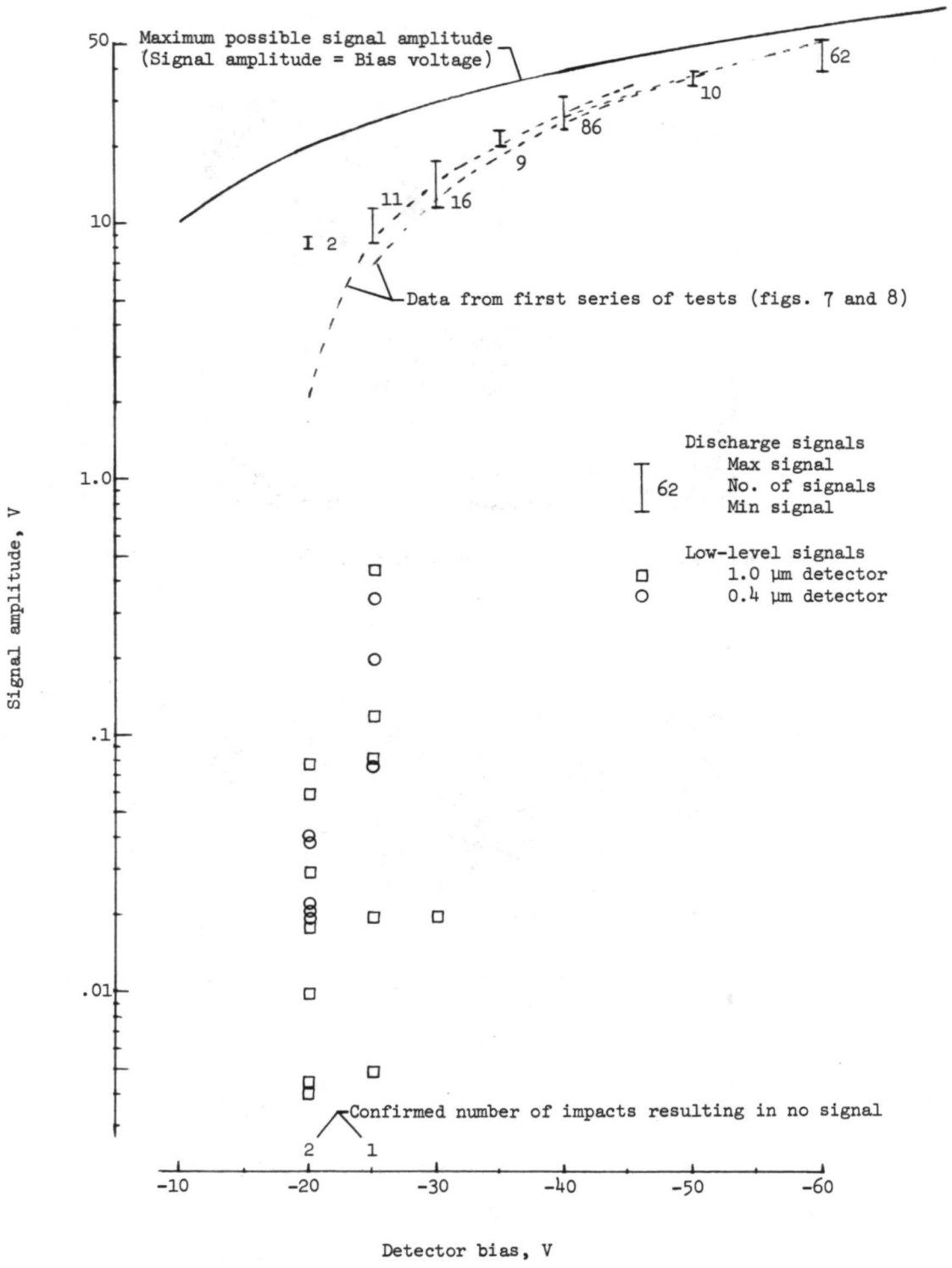

Figure 15.- Signal amplitude versus detector bias voltage. Tests 18 to 36.

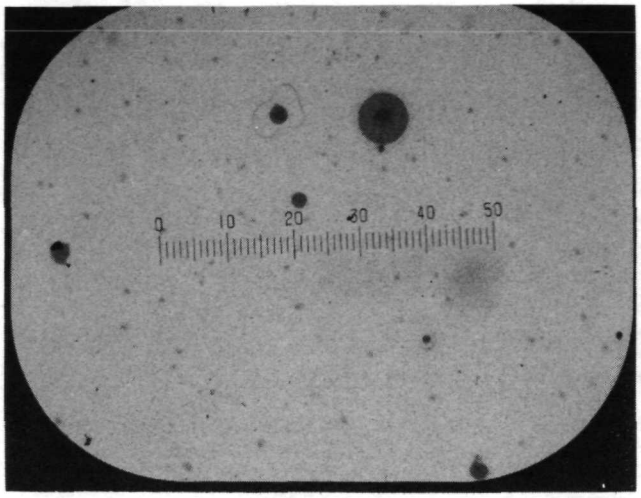

(a) Impact-signal craters for discharge and low-level signals. Test 32; bias, -20 V.

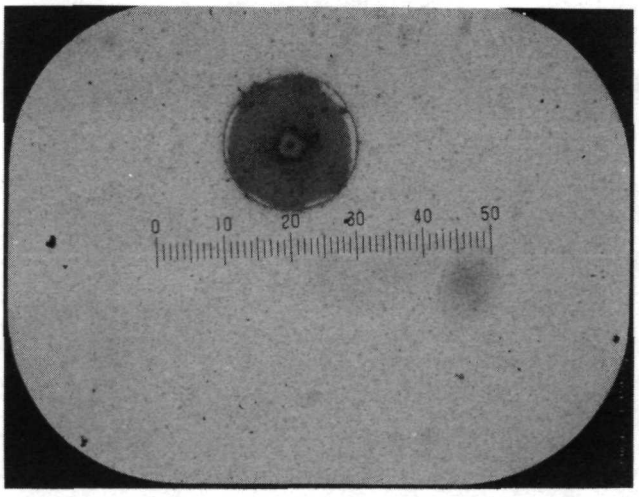

L-73-6828

(b) Impact-signal crater for discharge signal. Test 26; bias, -60 V.

Figure 16.- Photomicrographs of impact sites on a sintered detector. Scale: 1 division = 2.5 μm; 1.0-μm detector.

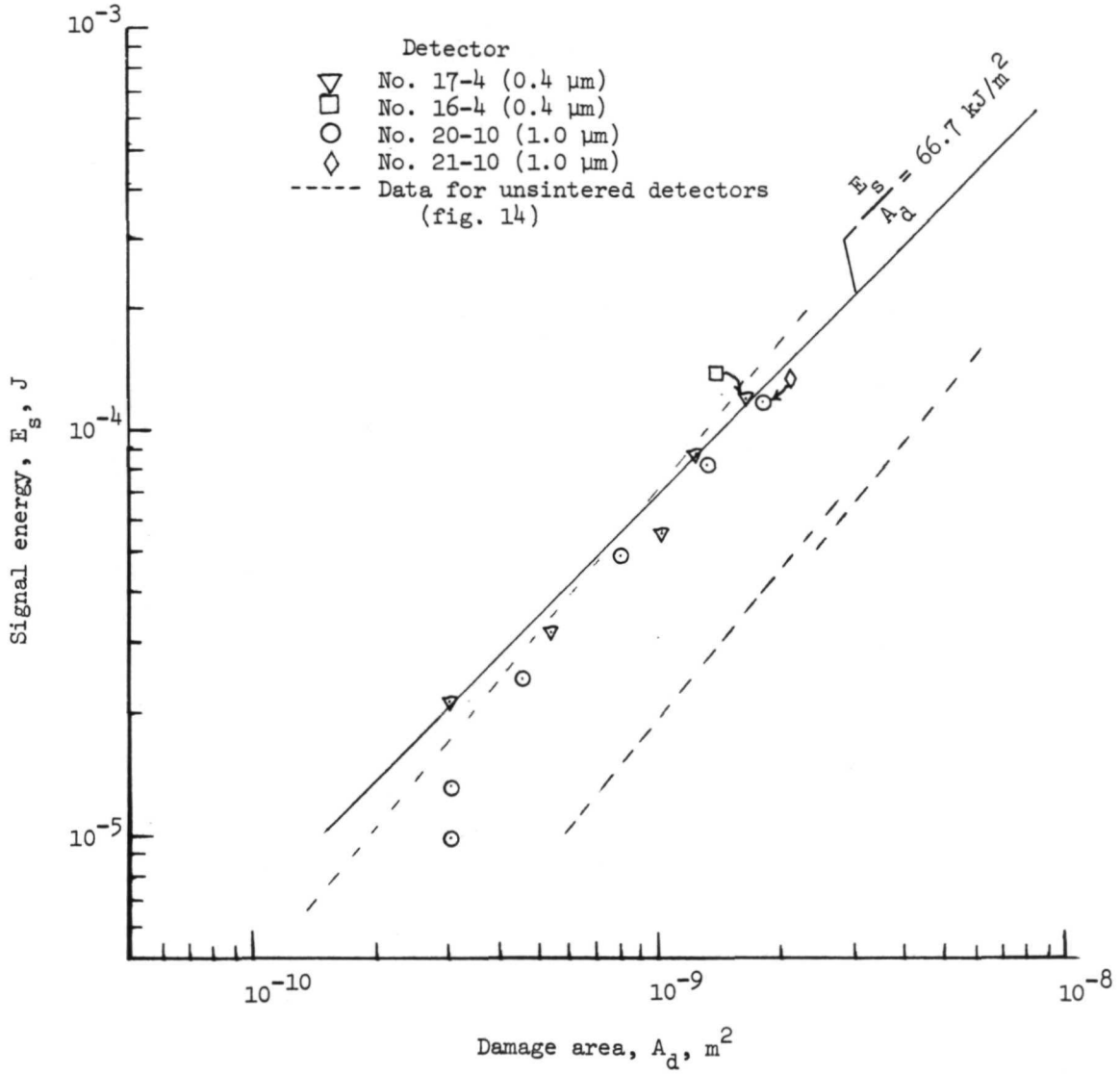

Figure 17.- Correlation of signal energy with damage area at the impact site for sintered detectors. Tests 18 to 36.

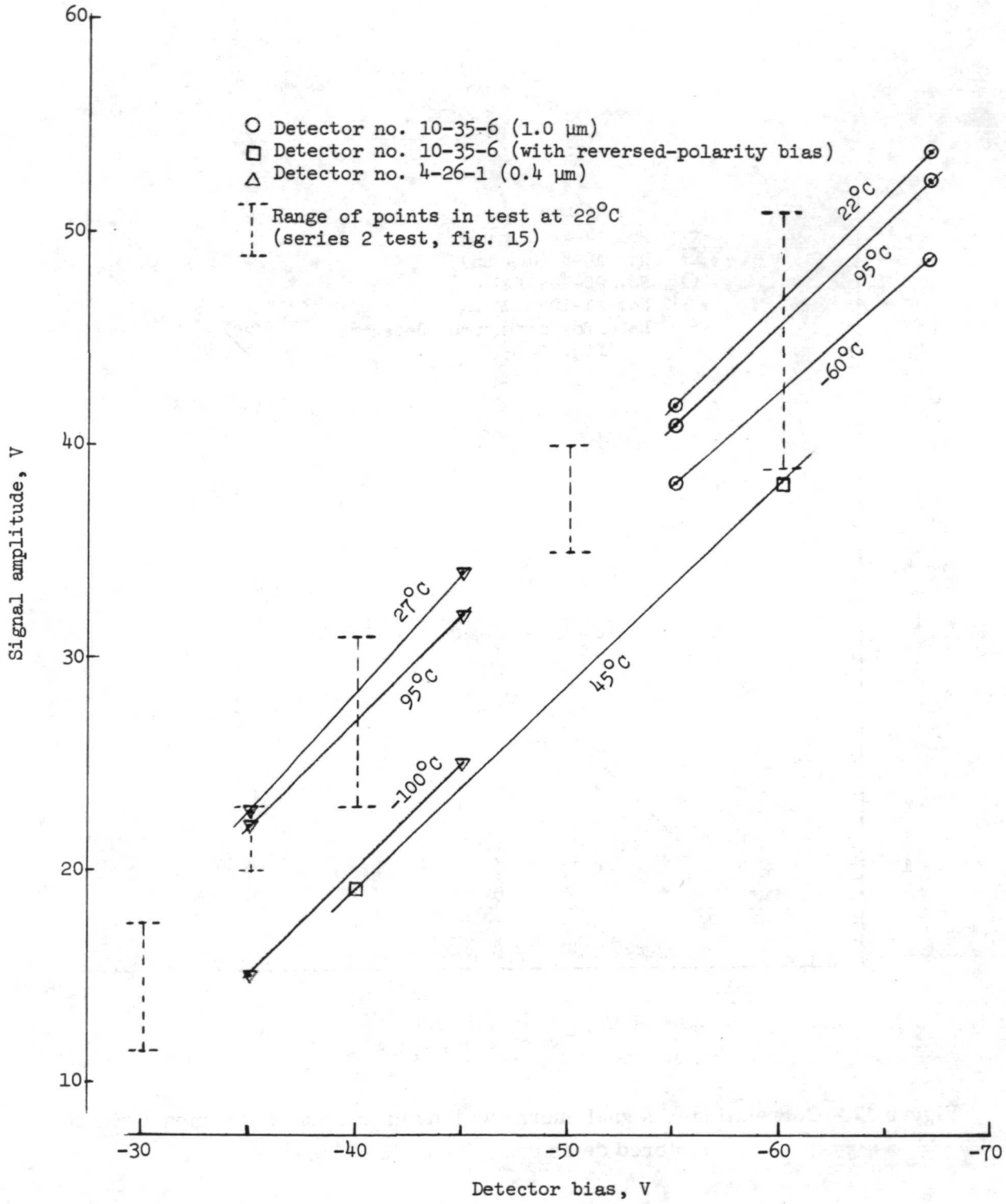

Figure 18.- Signal amplitude versus detector bias voltage for impacts at temperatures between 95° and -100° C.

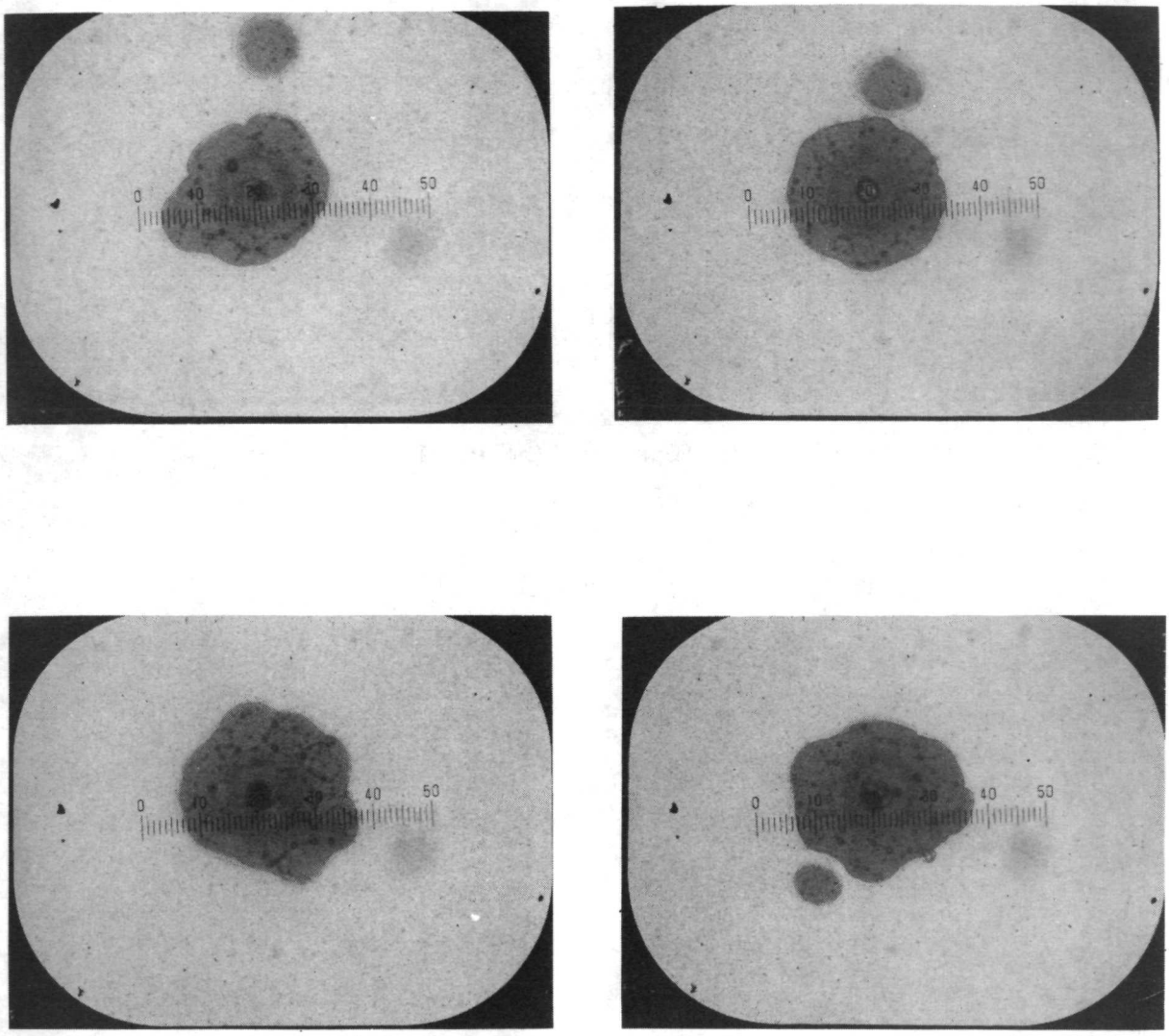

Figure 19.- Photomicrographs of impact-signal craters with detector temperature at -60° C. Scale: 1 division = 2.5 μm; bias, -67 V; 1.0-μm detector.

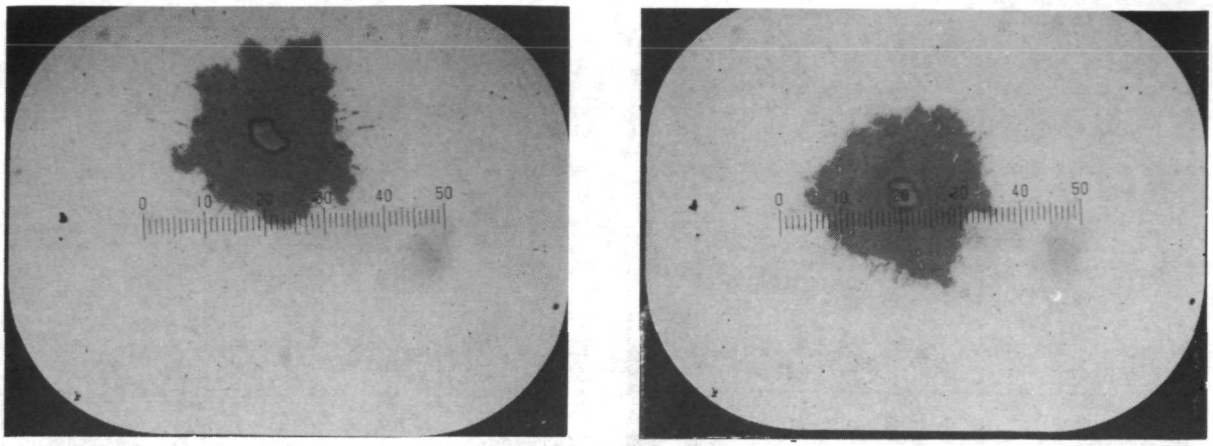

(a) Bias, 60 V (positive).

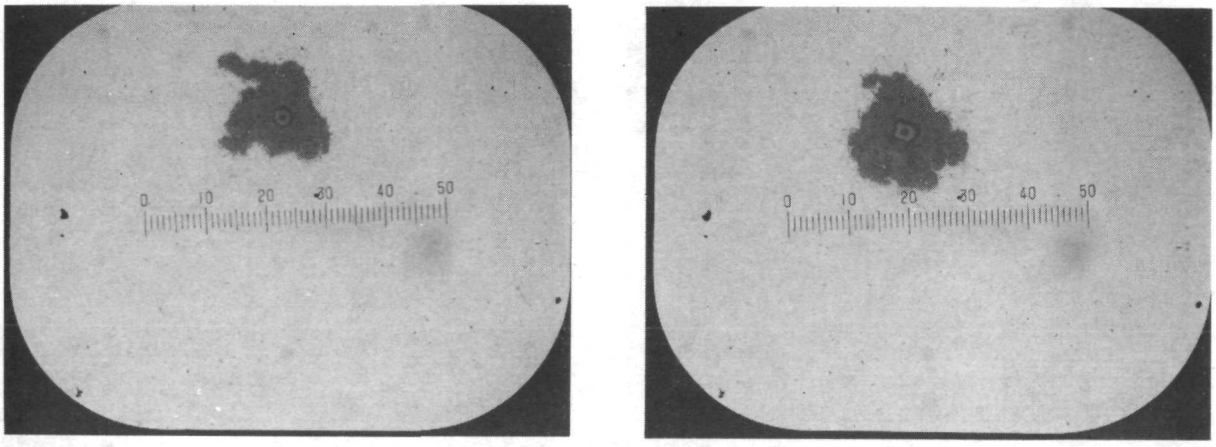

L-73-6830

(b) Bias, 40 V (positive).

Figure 20.- Photomicrographs of impact-signal craters with positive polarity on Si electrode. Scale: 1 division = 2.5 μm; 1.0-μm detector.

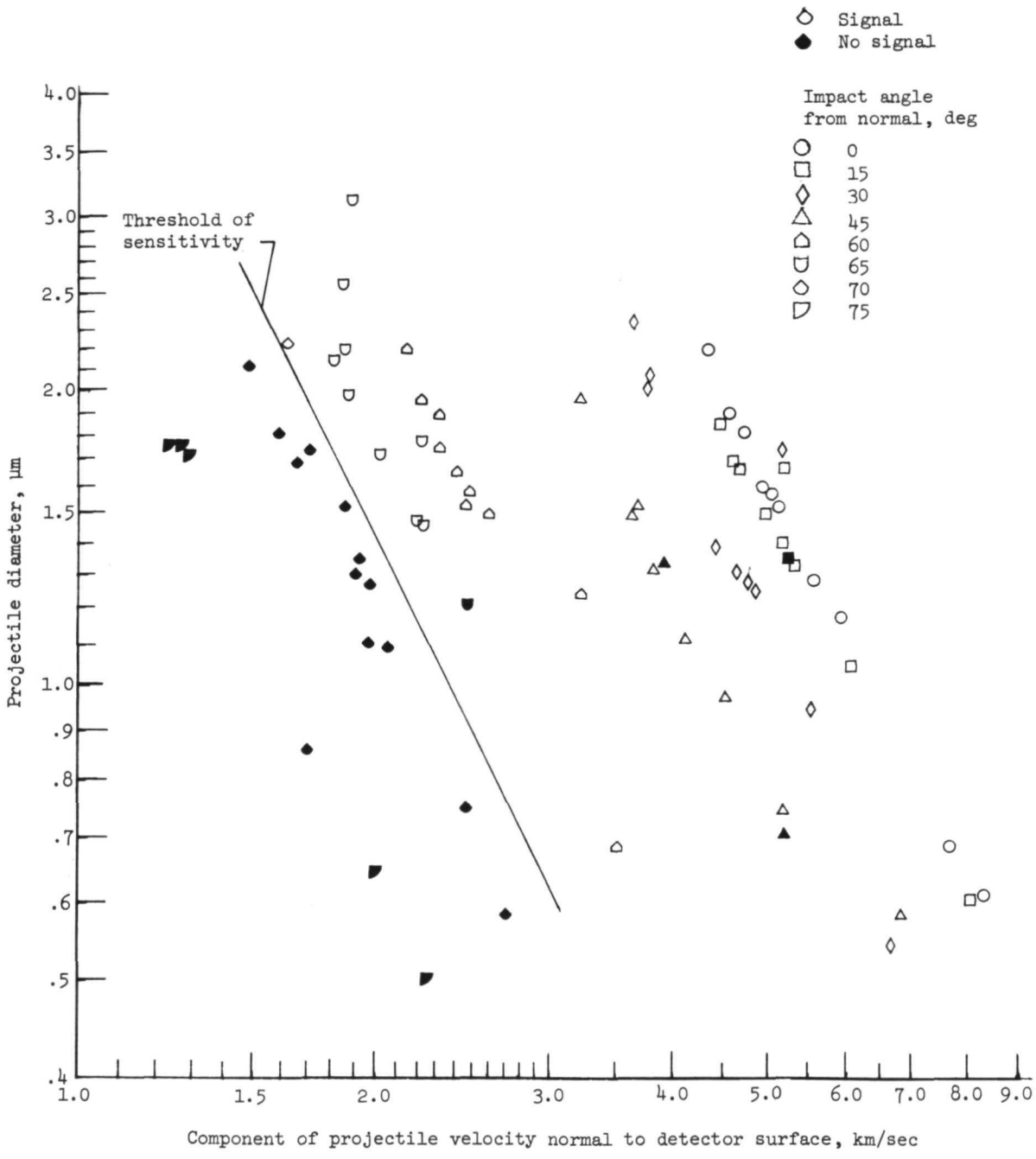

Figure 21.- Response of a 1.0-μm detector relative to projectile diameter and component of velocity normal to detector surface.

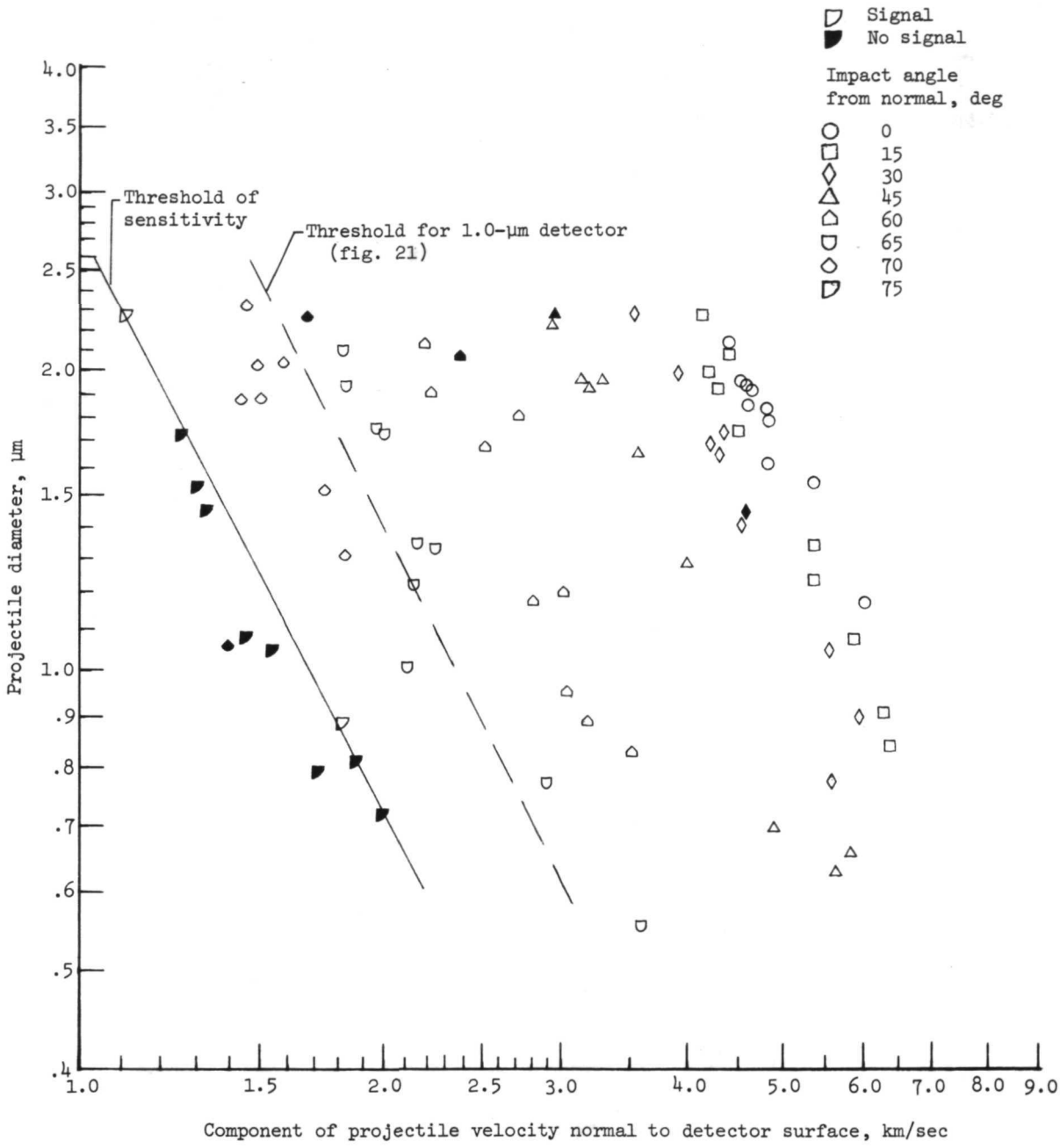

Figure 22.- Response of a 0.4-μm detector relative to projectile diameter and component of velocity normal to detector surface.

NASA-Langley, 1973 —— 32 L-8962

NATIONAL AERONAUTICS AND SPACE ADMINISTRATION
WASHINGTON, D.C. 20546

OFFICIAL BUSINESS
PENALTY FOR PRIVATE USE $300

SPECIAL FOURTH-CLASS RATE BOOK

POSTAGE AND FEES PAID
NATIONAL AERONAUTICS AND SPACE ADMINISTRATION
451

U.S.MAIL

POSTMASTER: If Undeliverable (Section 158 Postal Manual) Do Not Return

"The aeronautical and space activities of the United States shall be conducted so as to contribute . . . to the expansion of human knowledge of phenomena in the atmosphere and space. The Administration shall provide for the widest practicable and appropriate dissemination of information concerning its activities and the results thereof."

—NATIONAL AERONAUTICS AND SPACE ACT OF 1958

NASA SCIENTIFIC AND TECHNICAL PUBLICATIONS

TECHNICAL REPORTS: Scientific and technical information considered important, complete, and a lasting contribution to existing knowledge.

TECHNICAL NOTES: Information less broad in scope but nevertheless of importance as a contribution to existing knowledge.

TECHNICAL MEMORANDUMS: Information receiving limited distribution because of preliminary data, security classification, or other reasons. Also includes conference proceedings with either limited or unlimited distribution.

CONTRACTOR REPORTS: Scientific and technical information generated under a NASA contract or grant and considered an important contribution to existing knowledge.

TECHNICAL TRANSLATIONS: Information published in a foreign language considered to merit NASA distribution in English.

SPECIAL PUBLICATIONS: Information derived from or of value to NASA activities. Publications include final reports of major projects, monographs, data compilations, handbooks, sourcebooks, and special bibliographies.

TECHNOLOGY UTILIZATION PUBLICATIONS: Information on technology used by NASA that may be of particular interest in commercial and other non-aerospace applications. Publications include Tech Briefs, Technology Utilization Reports and Technology Surveys.

Details on the availability of these publications may be obtained from:

SCIENTIFIC AND TECHNICAL INFORMATION OFFICE

NATIONAL AERONAUTICS AND SPACE ADMINISTRATION

Washington, D.C. 20546